Politechnika Warszawska

WYDZIAŁ FIZYKI

Bachelor's diploma thesis

na kierunku Fizyka Techniczna
w specjalności Fizyka Komputerowa

Analysis of angular correlations of protons with Φ mesons in proton-proton collisions in the ALICE experiment

Zuzanna Chochulska
Numer albumu: 305000

promotor:
dr inż. Łukasz Graczykowski

WARSZAWA 2023

CERN-THESIS-2023-012
31/01/2023

Streszczenie

Tytuł pracy: Analiza korelacji kątowych protonów z mezonami Φ w zderzeniach proton-proton w eksperymencie ALICE.

Dwucząstkowe korelacje kątowe pozwalają na badanie mechanizmów hadronizacji. Podczas tego procesu z kwarków i gluonów powstają hadrony. Proces hadronizacji ciągle nie został w pełni poznany. Jednym z wielu zaproponowanych modeli teoretycznych do jego opisu jest strunowy model Lund. Jest on wykorzystywany w generatorze Monte Carlo PYTHIA.

Korelacje kątowe są funkcją dwóch zmiennych: różnicy pseudospieszności $\Delta\eta = \eta_1 - \eta_2$ i różnicy kąta azymutalnego $\Delta\varphi = \varphi_1 - \varphi_2$. Korelacje te są czułe na różne mechanizmy hadronizacji. Celem analiz korelacji kątowych jest zrozumienie mechanizmu powstawania cząstek, poprzez rozłożenie ich na czynniki i zrozumienie wkładu pochodzącego z różnych źródeł. Dla wszystkich zbadanych do tej pory par barion-barion oraz antybarion-antybarion w okolicy $\Delta\eta\Delta\varphi = (0{,}0)$ otrzymano antykorelację, natomiast dla mezonów typowo otrzymuje się charakterystyczny pik. Analiza korelacji kątowych $p - \Phi$ mogłaby umożliwić na odpowiedzenie na pytanie czy antykorelacja otrzymywana dla wszystkich zbadanych do tej pory par barion-barion oraz antybarion-antybarion w okolicy $\Delta\eta\Delta\varphi = (0{,}0)$ jest efektem, na który wpływ ma masa. Wspomniana wcześniej antykorelacja nie jest przewidywana przez żaden z modeli teoretycznych, co oznacza, że nie uwzględniają one wszystkich efektów mających miejsce w tym procesie. Analiza systemu $p - \Phi$ dałaby fizykom teoretycznym dodatkowy pomiar, umożliwiający poprawę wykorzystywanych modeli.

Głównym celem pracy inżynierskiej jest stworzenie modułu do nowego oprogramowania O^2 wykorzystywanego w eksperymencie ALICE w CERNie, który pozwoli na otrzymanie funkcji korelacji kątowej protonów z mezonami Φ w zderzeniach pp. Wprowadzenie nowego oprogramowania było niezbędne ze względu na zmianę trybu akwizycji danych w eksperymencie podczas Run 3. Kod AliFemto, wykorzystywany w poprzednim oprogramowaniu AliROOT/AliPhysics nie może być dalej używany, ze względu na znaczące zmiany w formacie danych i formie wykonywanych analiz w oprogramowaniu O^2. W celu wykonania tej pracy musiałam więc od początku napisać narzędzie do analizy. Całą pracę podzielić można było na dwie główne części. Pierwszą z nich było rozwinięcie oprogramowania, tak by możliwe było zrekonstruowanie mezonów Φ. Była to część typowo inżynierska i musiała być praktycznie sfinalizowana przed rozpoczęciem pracy nad drugą częścią, którą było badanie korelacji zidentyfikowanych hadronów z mezonami Φ.

Słowa kluczowe:
CERN, ALICE, korelacje kątowe, hadronizacja

(czytelny podpis opiekuna naukowego) (czytelny podpis dyplomanta)

Abstract

Thesis title: Analysis of angular correlations of protons with Φ mesons in proton-proton collisions in the ALICE.

Two-particle angular correlations allow the study of hadronization mechanisms. During this process hadrons are formed from quarks and gluons. The hadronization process is still not fully understood. One of the many theoretical models proposed to describe it is the Lund string model. It is used in the Monte Carlo generator PYTHIA.

The angular correlations are a function of two variables: the difference in pseudorapidity $\Delta\eta = \eta_1 - \eta_2$ and the difference in azimuthal angle $\Delta\varphi = \varphi_1 - \varphi_2$. These correlations are sensitive to different hadronization mechanisms. The goal of angular correlation analyses is to understand the mechanism of particle formation by decomposing the particles and understanding the contributions from different sources. For all baryon-baryon and antibaryon-antibaryon pairs studied so far, an anticorrelation is obtained in the vicinity of $\Delta\eta\Delta\varphi = (0{,}0)$, while a characteristic peak is typically obtained for mesons. Analysis of the angular correlations of $p - \Phi$ could make it possible to answer the question of whether the anticorrelation obtained for all the baryon-baryon and antibaryon-antibaryon pairs studied so far in the vicinity of $\Delta\eta\Delta\varphi = (0{,}0)$ is an effect influenced by mass. The previously mentioned anticorrelation is not predicted by any of the theoretical models, which means that they do not account for all the effects taking place in this process. Analysis of the $p - \Phi$ system would give theoretical physicists an additional measurement to improve the models used.

The main objective of the engineering work is to develop a module for the new O^2 software used in the ALICE experiment at CERN, which will allow to obtain the angular correlation function of protons with mesons Φ in pp collisions. The introduction of the new framework was necessary due to the change of the data acquisition mode in the experiment during Run 3. The AliFemto code used in the previous AliROOT/AliPhysics software can no longer be used, due to significant changes in the format of the data and the form of analysis performed in the O^2 framework. In order to do this work, I had to write an analysis tool from scratch. The whole work could be divided into two main parts. The first was to develop the software so that O^2 mesons could be reconstructed. This was a purely engineering part and the practical part had to be finalized before I could start working on the second part, namely studying the correlation of identified hadrons with Φ mesons.

Keywords
CERN, ALICE, angular correlations, hadronization

(supervisor's signature) (student's signature)

Oświadczenie o samodzielności wykonania pracy

Politechnika Warszawska

Zuzanna Chochulska
305000
Fizyka Techniczna

Oświadczenie

Świadoma odpowiedzialności karnej za składanie fałszywych zeznań oświadczam, że niniejsza praca dyplomowa została napisana przeze mnie samodzielnie, pod opieką kierującego pracą dyplomową.

Jednocześnie oświadczam, że:

- niniejsza praca dyplomowa nie narusza praw autorskich w rozumieniu ustawy z dnia 4 lutego 1994 roku o prawie autorskim i prawach pokrewnych (Dz.U. z 2006 r. Nr 90, poz. 631 z późn. zm.) oraz dóbr osobistych chronionych prawem cywilnym,
- niniejsza praca dyplomowa nie zawiera danych i informacji, które uzyskałem/-am w sposób niedozwolony,
- niniejsza praca dyplomowa nie była wcześniej podstawą żadnej innej urzędowej procedury związanej z nadawaniem dyplomów lub tytułów zawodowych,
- wszystkie informacje umieszczone w niniejszej pracy, uzyskane ze źródeł pisanych i elektronicznych, zostały udokumentowane w wykazie literatury odpowiednimi odnośnikami,
- znam regulacje prawne Politechniki Warszawskiej w sprawie zarządzania prawami autorskimi i prawami pokrewnymi, prawami własności przemysłowej oraz zasadami komercjalizacji.

Warszawa, dnia 20.01.2023 r.

(czytelny podpis dyplomanta)

Oświadczenie o udzieleniu Uczelni licencji do pracy

Politechnika Warszawska

Zuzanna Chochulska
305000
Fizyka Techniczna

Oświadczam, że jako autor pracy dyplomowej pt. *Analiza korelacji kątowych protonów z mezonami* Φ *w zderzeniach proton-proton w eksperymencie ALICE* udzielam[1] Politechnice Warszawskiej nieodpłatnej licencji na niewyłączne, nieograniczone w czasie, umieszczenie pracy dyplomowej w elektronicznych bazach danych oraz udostępnianie pracy dyplomowej w zamkniętym systemie bibliotecznym Politechniki Warszawskiej osobom zainteresowanym.

Licencja na udostępnienie pracy dyplomowej nie obejmuje wyrażenia zgody na wykorzystywanie pracy dyplomowej na żadnym innym polu eksploatacji, w szczególności kopiowania pracy dyplomowej w całości lub w części, utrwalania w innej formie czy zwielokrotniania.

Warszawa, dnia 20.01.2023 r. (czytelny podpis dyplomanta)

[1] Na podstawie Ustawy z dnia 27 lipca 2005 r. Prawo o szkolnictwie wyższym (Dz.U. 2005 nr 164 poz. 1365) Art. 239. oraz Ustawy z dnia 4 lutego 1994 r. o prawie autorskim i prawach pokrewnych (Dz.U. z 2000 r. Nr 80, poz. 904, z późn. zm.) Art. 15a. "Uczelni w rozumieniu przepisów o szkolnictwie wyższym przysługuje pierwszeństwo w opublikowaniu pracydyplomowej studenta. Jeżeli uczelnia nie opublikowała pracy dyplomowej w ciągu 6 miesięcy od jej obrony, student, który ją przygotował, może ją opublikować, chyba ze praca dyplomowa jest częścią utworu zbiorowego."

Contents

Chapter 1. Introduction . . . 13

1.1. Choice of observables . . . 14

1.2. Angular correlation function . . . 16

Chapter 2. Experimental setup . . . 19

2.1. CERN . . . 19

2.2. LHC . . . 19

2.3. ALICE . . . 21

2.3.1. VZERO . . . 21

2.3.2. Inner Tracking System (ITS) . . . 22

2.3.3. Time Projection Chamber (TPC) . . . 22

2.3.4. Time-of-Flight (TOF) . . . 23

2.4. GRID . . . 23

Chapter 3. Software environment . . . 25

3.1. Introduction to O^2 the framework . . . 25

3.2. The O^2 data format . . . 25

3.3. FemtoWorld – the new O^2 module . . . 27

3.4. Hyperloop train system . . . 29

Chapter 4. Data analysis . . . 31

4.1. Data sample . . . 31

4.2. Proton candidate selection 31

4.3. Φ candidate selection 34

Chapter 5. Results 39

Chapter 6. Summary and conclusions 41

Bibliography 43

List of Figures 45

List of Tables 49

Appendix A. Comparison of angular correlation $\pi - \Phi$ with angular correlation $p - \Phi$ 51

A.1. Angular correlation function for $\pi - \Phi$ 51

A.2. Angular correlation function for $p - \Phi$ 54

Chapter 1

Introduction

Particle physics focuses on understanding the most basic constituents of matter of the world around us and the interactions between them [1]. Fundamental particles are those that have no internal structure, at least to the extent of current knowledge. The use of high energy collisions in this field of study is therefore crucial, as it makes the resolution with which subatomic particles are studied much higher. The resolution with which measurement is possible is limited by the de Broglie wavelength of these fundamental particles, which is given by the equation:

$$\lambda = \frac{\mathrm{h}}{p}, \tag{1.1}$$

where h is the Planck's constant and p is the beam momentum. As a result, beams with higher momentum have a shorter length, which leads to their higher resolution. The second key factor because of which high energies are used is that this is necessary to create particles that are often heavy and do not exist under normal conditions in nature [2].

There are many facilities that have been conducting particle physics experiments over the years. One such facility is the Large Hadron Collider (LHC) at CERN on the French-Swiss border near Geneva. It is the largest and most powerful particle accelerator in the world and it is used to collide protons and heavy ions at high energies, which allows scientists to study the properties of fundamental particles and their interactions.

One of the experiments located at the LHC is ALICE (A Large Ion Collider Experiment). It is designed to research the physics of heavy ion collisions. As such, it is a detector whose main purpose is to investigate the physics of heavy ions. This enables the study of quark-gluon plasma [3, 4], the state of matter in the early universe, just about a few millionths of a second after the Big Bang, in which quarks and gluons are in a deconfined form. Taking into account the amazing ability to identify particles and reliable tracking for low p_T, the ALICE experiment allows for a unique quality of measurements.

Hadronization is the process through which quarks and gluons combine to form hadrons. This process has not been fully understood and it can be only described in a non-perturbative way.

This means that it cannot be derived from the first principles of physics. Because of that, phenomenological models are being used. One of the most popular models is the Lund string model [5]. It treats most gluons, except those of very high energies, as field lines that form strings. Certain parameters of the phenomenological models need to be constrained from experimental data. Analysis of the $p - \Phi$ system, which has not been studied before, would give theoretical physicists an additional measurement to improve the models used.

The observable that makes it possible to study contributions from different mechanisms of particle production is the angular correlation function. The $\Delta\eta\Delta\varphi$ distributions are sensitive to different physics phenomena, one of them being hadronization mechanisms. The study aims to understand particle production's mechanism by decomposing the correlations into factors and understanding the contributions from different sources. A typical correlation function has a peak for $\Delta\eta\Delta\varphi = (0,0)$ and a ridge for $\Delta\varphi = 0$ [6].

The angular correlation graphs obtained so far for baryon-baryon and antibaryon-antibaryon pairs in the vicinity of $\Delta\eta\Delta\varphi$ = (0,0) had a strong anticorrelation. Which is surprising given the shape of a typical correlation function. This effect is not predicted by any of the theoretical models. This means that they do not take into account all of the effects that are involved in the hadronization process. The lightest pair of baryon-baryon and antibaryon-antibaryon, for which anticorrelation was obtained, was p–p and $\hbar p - \hbar p$. By correlating a meson, with a mass close to that of a proton, we can test if this effect is related to the mass. The most abundant meson that meets these criteria is the Φ meson. This hypothesis has not been tested before.

The primary focus of the work was to develop the software for the completely new O^2 system used in the ALICE experiment at CERN in a way that would make it possible to obtain angular correlation functions for Φ mesons with identified hadrons, in particular protons. The work can be divided into two phases. The first stage was to build a module for the O^2 software used at CERN to reconstruct Φ mesons. The second step was to study the angular correlations of the identified hadrons with the mesons Φ. In order to be able to analyze the angular correlations, it was necessary to complete the first stage of the work. Obtaining the results of this thesis involved writing most of the analysis software from scratch.

The ALICE software is new and is constantly being developed by many people. It required me to be familiar with C++ version 17, which I had not had the opportunity to learn during my time at university. I also had to learn how to use the GitHub version control system. This was a key and essential tool used in this work, due to the fact that the ALICE framework is developed by people all over the world at the same time. This analysis was performed using GRID [7].

1.1. Choice of observables

This section introduces the basic observables that are key to understanding angular correlations, which are also explained in greater detail in this chapter.

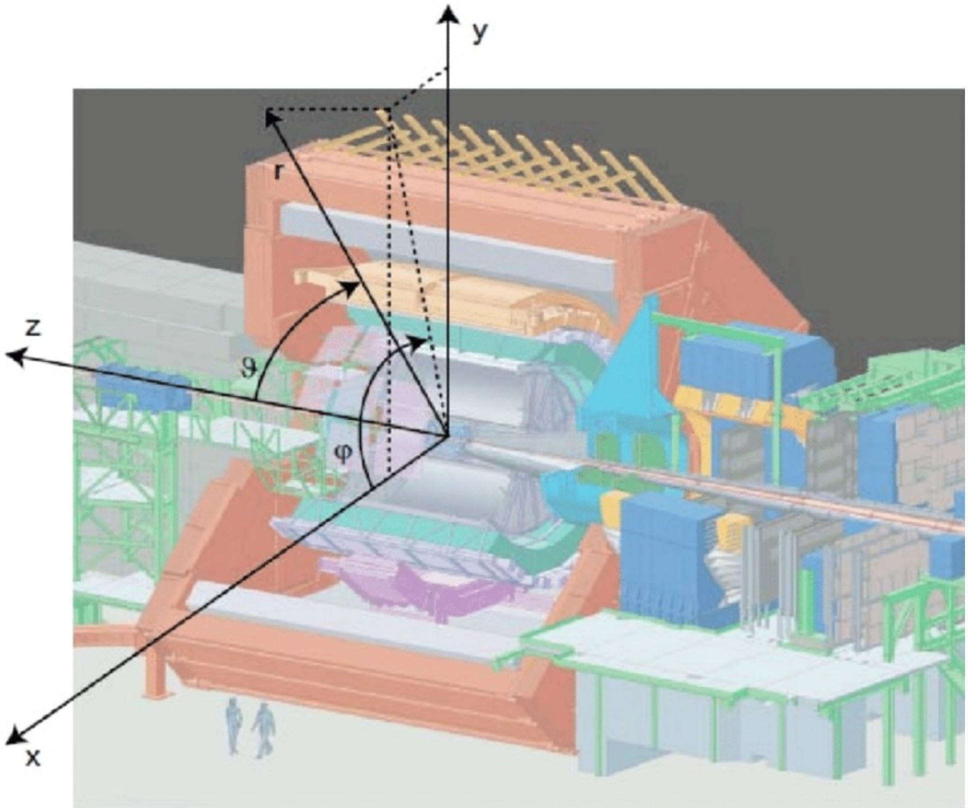

Figure 1.1: Definition of the polar angle θ and the azimuthal angle φ [8].

Azimuthal angle

The azimuthal angle φ is the angle between the transverse momentum vector p_T and the positive x-axis. The coordinate system in relation to the geometry of the ALICE detector is defined in figure 1.1.

Pseudorapidity

Pseudorapidity is a simplified version of rapidity, as it depends only on the polar angle. In this case, we use a value similar to rapidity but simplified. Pseudorapidity is a good approximation of rapidity only in the midrapidity range. Pseudorapidity is an observable often used to determine the angle of a particle with respect to the beam axis. It is defined as:

$$\eta = -\ln\left[\tan\left(\frac{\theta}{2}\right)\right]. \tag{1.2}$$

Figure 1.1 determines the coordinate system in which the polar angle θ and the azimuthal angle φ are shown.

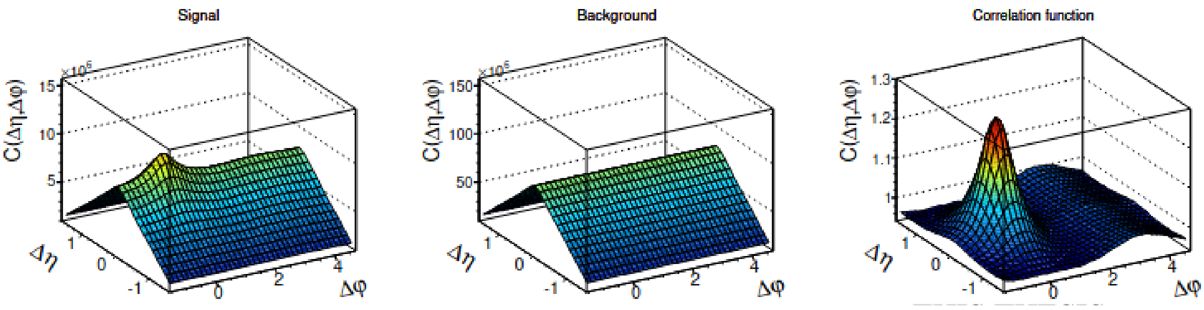

Figure 1.2: Construction of the $\Delta\eta\Delta\varphi$ correlation function. Signal distribution (left), background distribution (middle), and correlation function (right) [9]

.

1.2. Angular correlation function

Angular correlation functions are obtained by dividing the signal distribution by the background distribution. It is defined as:

$$C\left(\Delta\eta,\Delta\varphi\right)=\frac{N_{pairs}^{mixed}}{N_{pairs}^{signal}}\frac{S(\Delta\eta,\Delta\varphi)}{B(\Delta\eta,\Delta\varphi)}, \tag{1.3}$$

where $S(\Delta\eta,\Delta\varphi)$ is a signal distribution and $B(\Delta\eta,\Delta\varphi)$ is a background distribution. The signal distribution is produced from pairs of particles from the same event. The background distribution is constructed using the procedure of event mixing, where each particle in the pair comes from a different event. An example of a signal distribution, background distribution, and correlation function is shown in figure 1.2.

Angular correlations give a visual representation of the full landscape of correlations. They are particularly sensitive to contributions from different sources. The study aims to decompose angular correlations into components, making it possible to quantify the contribution of each source. The components that comprise the angular correlation are shown in figure 1.3. Figure 1.4 shows the angular correlation function for selected identified hadrons of the same and opposite electric signs. The graphs were obtained from experimental data from pp collisions at 7 TeV energy recorded by the ALICE experiment during the LHC Run 1. In the plots for pions mesons and kaons, we note the similar shape of the angular correlation function for particles of both the same sign, as well as those of the opposite sign. However, on the graph for protons, we notice a strong anticorrelation in the vicinity of $(\Delta\eta,\Delta\varphi)=(0{,}0)$.

By comparing experimental data with theoretical models, we get the following results shown in figure 1.5 for like-sign particles and in figure 1.6 for the unlike-sign ones. Thus, as can be seen, theoretical models do not predict the anti-correlation that is measured. The anticorrelation for baryon pairs was first discovered in the 1980s [12]. At the time, it was thought to be caused by local conservation of the baryon number. To make the correlation positive for $\Delta\eta\Delta\varphi=(0{,}0)$ in one jet we would need to produce at least two baryons. Therefore, we need to produce two baryons and

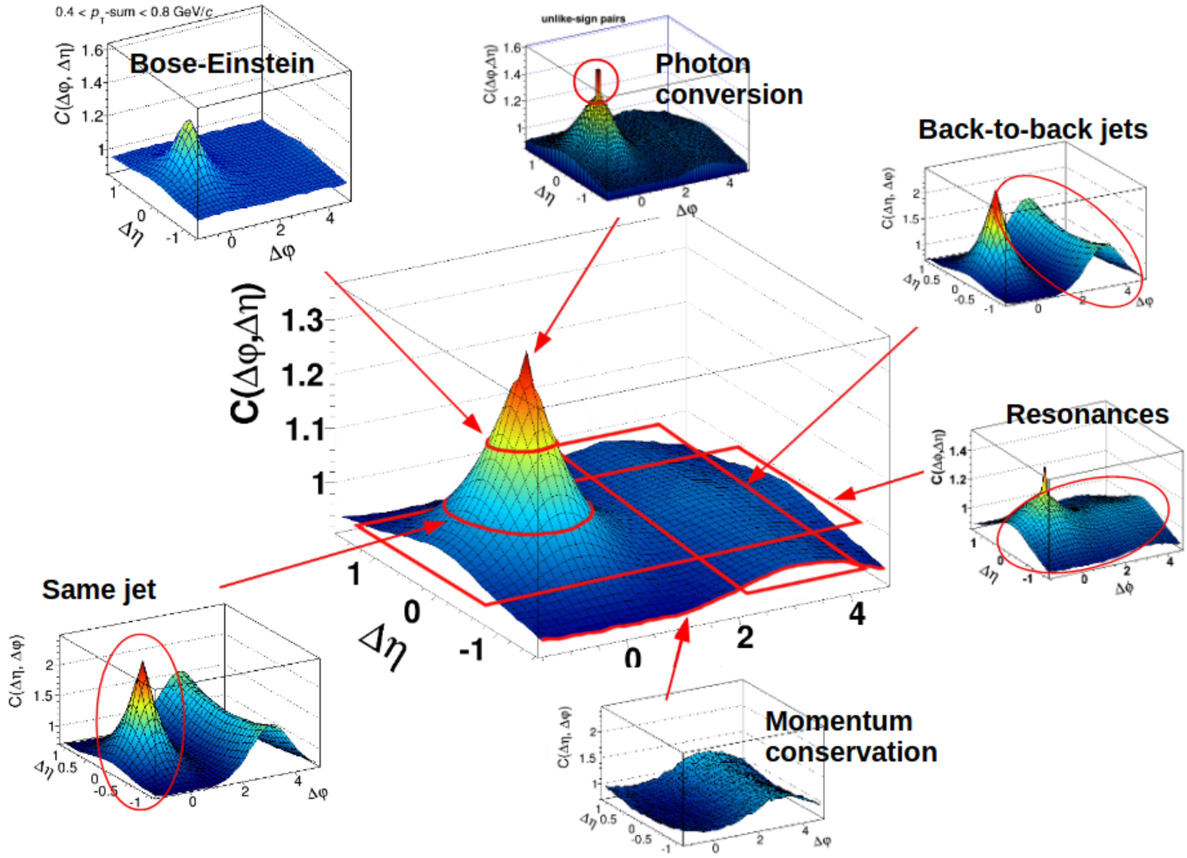

Figure 1.3: The components that comprise the angular correlation [10].

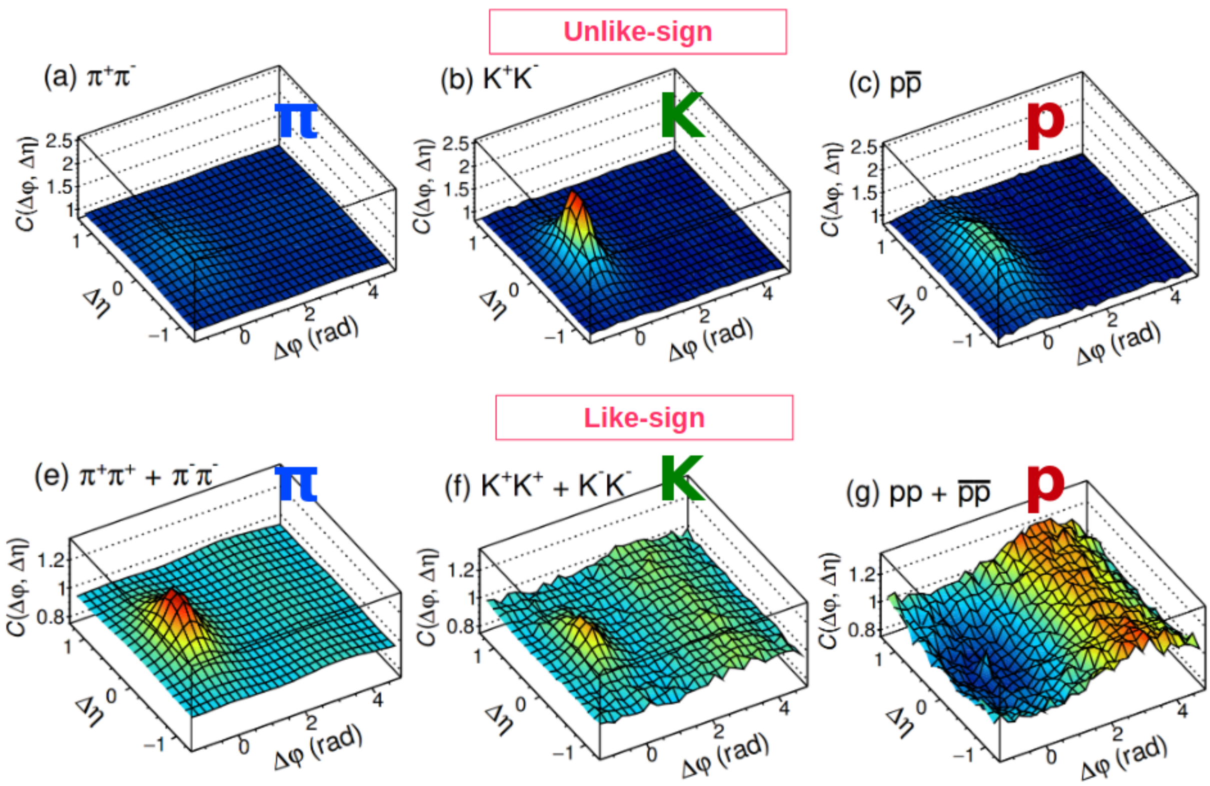

Figure 1.4: Correlation function C(Δη, Δφ) of unlike-sign and like-sign particles [9].

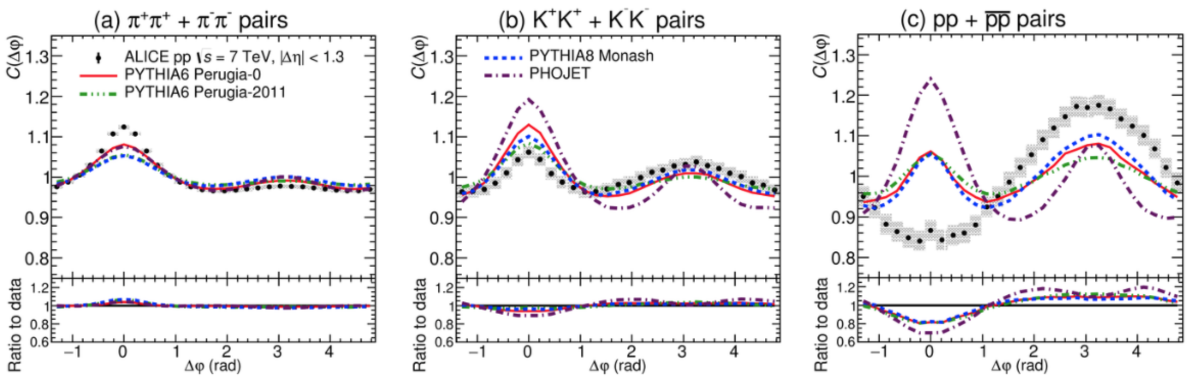

Figure 1.5: Comparison to MC models: like-sign [11].

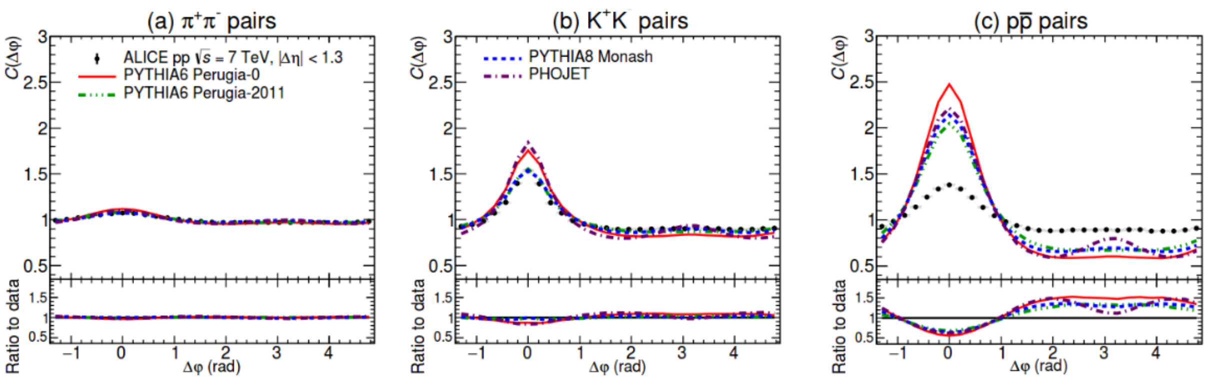

Figure 1.6: Comparison to MC models: unlike-sign [11].

two anti-baryons, to conserve local baryon number. One baryon has a mass of at least about 1 GeV. A minimum of 4 GeV is therefore required. At that time, the collisions reached an energy of 27 GeV. The 4 GeV of 27 GeV available was a much larger fraction than it is now at an energy of 13 TeV yet we still observe the exact same thing. Possible explanations for this phenomenon are:

- too small p_T range,
- Coulomb repulsion,
- Fermi-Dirac Quantum Statistics,
- Strong Final-State Interactions.

It should also be checked if this effect also exists for other baryons. It turns out that these explanations do not provide an answer to the received anticorrelation. Another explanation for this phenomenon could be the mass/energy considerations, since producing heavy particles is not favorable. The way to check that is to correlate a proton with a meson with a similar mass to it. The particle satisfying the given conditions is the Φ meson. The aim of this thesis is to obtain the angular correlation of protons with Φ mesons.

Chapter 2

Experimental setup

This chapter contains information dedicated to CERN in section 2.1, Large Hadron Collider (LHC) in section 2.2, ALICE experiment in section 2.3 and GRID in section 2.4.

2.1. CERN

CERN (Conseil Européen pour la Recherche Nucléaire) is a European research organization and it is at the forefront of the development of both fundamental particle physics research and technology development. The goal of physicists working at CERN is to understand what the world around us is made of and how it works. To achieve this, CERN allows scientists from around the world to collaborate on a globally unique range of accelerators [13]. This special environment allowed the discovery of the Higgs boson in 2012. Figure 2.1 depicts experiments and accelerators at CERN.

2.2. LHC

The Large Hadron Collider (LHC) is one of the most complex big science machines. It is the largest and most powerful particle accelerator in the world. It is a 27-kilometer-long ring, composed of superconducting magnets that curve the trajectory of the two high-energy beams that are made to collide. The beams collide at four experiments located at the LHC ring [15]:

- ATLAS (A Toroidal LHC ApparatuS) - a general-purpose detector that is used to study a wide range of physics phenomena,
- CMS (Compact Muon Solenoid) - a general-purpose detector, used to study a wide range of physics phenomena,
- LHCb (LHC-beauty) - is a specialized detector used to study the properties of particles containing bottom quarks,
- ALICE (A Large Ion Collider Experiment) - is a specialized detector, designed to study the properties of QGP.

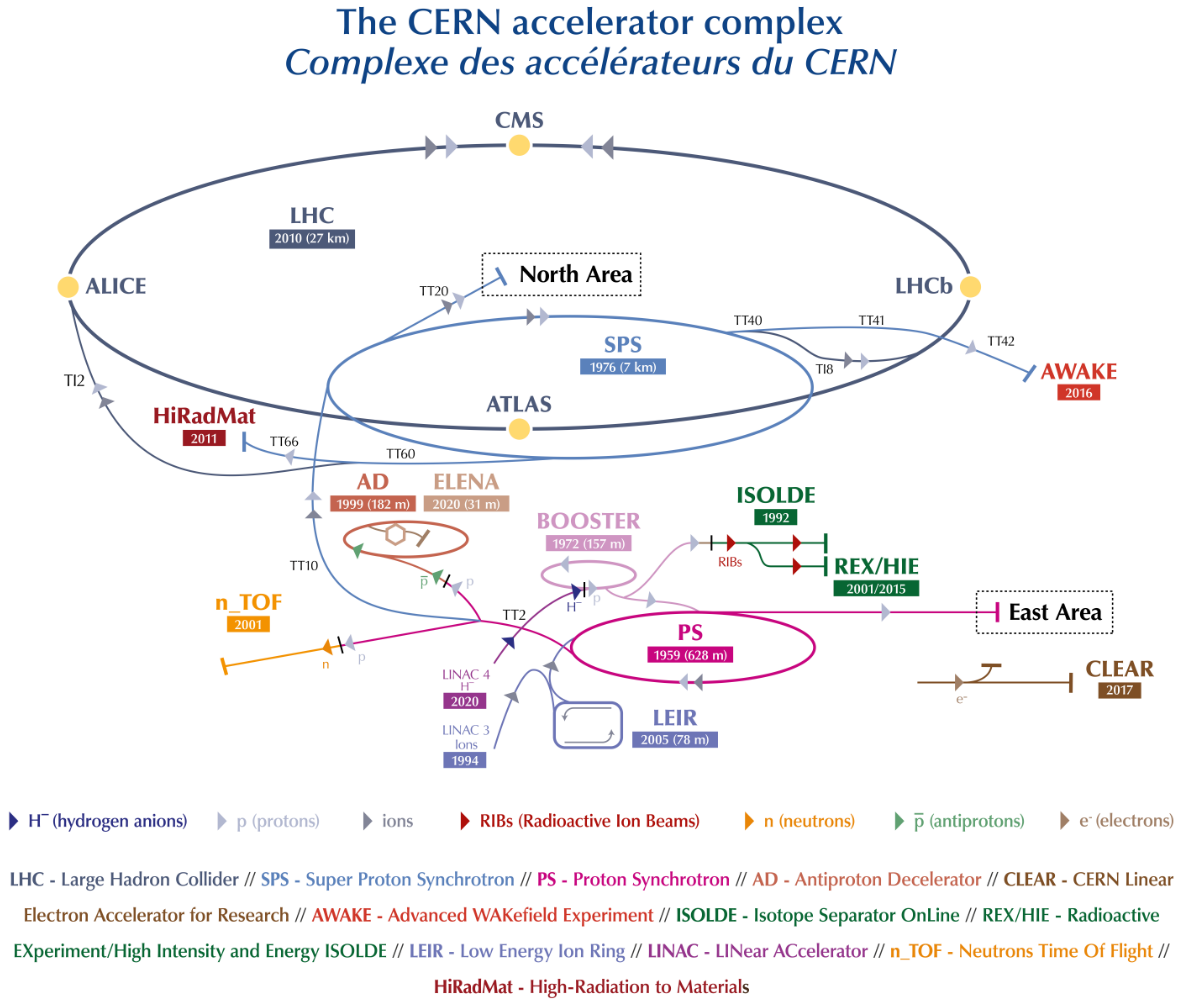

Figure 2.1: Experiments and accelerators at CERN [14].

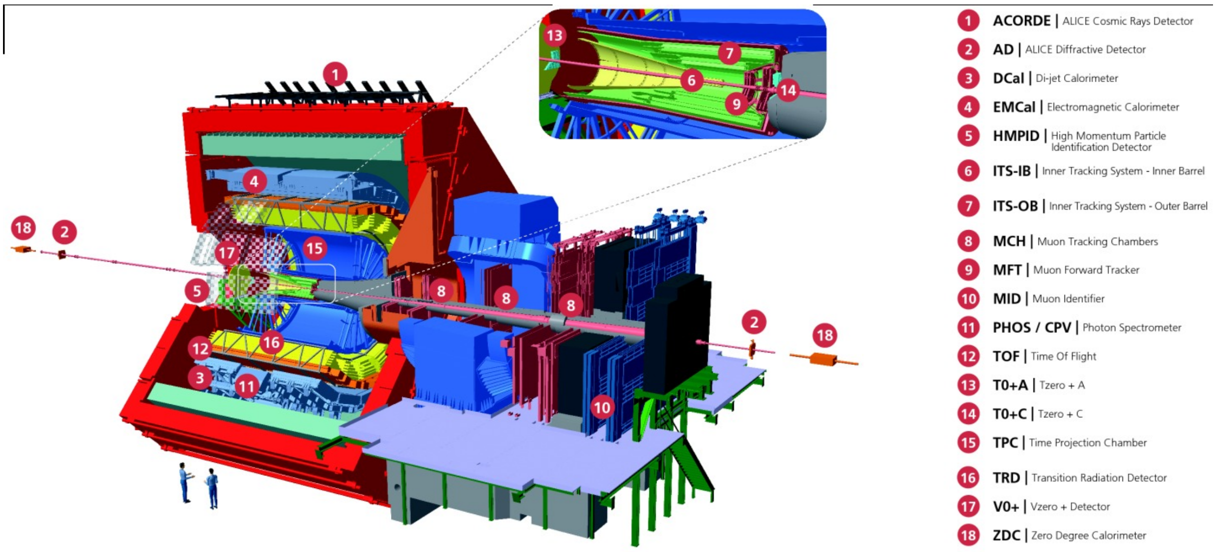

Figure 2.2: 3D ALICE schematics of ALICE detector after the upgrade for Run 3 [17].

2.3. ALICE

The ALICE [16] (A Large Ion Collider Experiment) Collaboration's aim is to investigate quark-gluon plasma (QGP) in a very small volume and very large energy density and high temperature. The ALICE experiment is the only CERN experiment dedicated to analyzing heavy ion collisions; however, it also studies pp and p–Pb interactions.
The ALICE detector consists of multiple sub-detectors. Each contributes the information necessary to correctly identify the particles tracked in the ALICE experiment. The sub-detectors that comprise the ALICE experiment are shown in figure 2.2.

Detectors that are particularly important for particle identification are *TPC* and *TOF* as described in section 2.3.3 and section 2.3.4 respectively. Particle identification (PID) used in this thesis is based on the N_σ method. It stands for the number of standard deviations of Gaussian distribution around theoretical signals. The theoretical signal for the TPC signal is a Bethe-Bloch formula (2.1), whereas for the TOF signal, it is an expected time of arrival. The ITS and TPC detectors are the main tracking devices in the ALICE experiment. The following sections 2.3.1 - 2.3.4 detail the VZERO, ITS, TPC, and TOF sub-detectors. The VZERO detector is responsible for measuring multiplicity, ITS for particle tracking, TPC, and TOF for particle identification.

2.3.1. VZERO

One of the subdetectors in the front regions of the ALICE detector is the VZERO system. It is also known as V0. The name VZERO is used to avoid confusion with the particle V0.

VZERO system consists of two arrays VZERO-A and VZERO-C at asymmetric positions. In the radial direction, each VZERO array is divided into four rings, and each ring is divided into eight sections in the azimuthal direction. Each of the 32 cells contains a scintillation counter, which counts the multiplicity of charged particles. Such measurement is based on the energy deposited in the scintillation detector and it is used to monitor LHC beam conditions and to measure basic physics quantities such as luminosity, centrality, and event plane direction in collisions [18].

2.3.2. Inner Tracking System (ITS)

Inner Tracking System (ITS) is a cylindrical-shaped silicon tracker. It consists of six layers surrounding the collision region. Each of the six layers consists of two layers of *Silicon Pixel Detectors* (SPD), *Silicon Drift Detectors* (SDD), and double-sided *Silicon Strip Detectors* (SSD). It plays a key role in ALICE data analysis, as it is contributing to the reconstruction of the primary interaction vertex, as well as improving the momentum and angular resolution of tracks reconstructed in the *TPC* [19].

The new Inner Tracking System 2 detector (ITS2), developed during Long Shutdown 2, considerably improves the resolution of collision parameters and tracking efficiency, in particular for low transverse momentum particles, along with data readout capabilities [20]. It only uses layers of pixel technology.

2.3.3. Time Projection Chamber (TPC)

One of the most important tracking detectors in the ALICE experiment is the *Time Projection Chamber* [21]. It uses a combination of electric fields and magnetic fields, combined with sensitive $Ne - Co_2 - N_2$ gas. It provides information on charged particles. Particles passing through the gas in the *TPC* detach electrons which drift toward the end plates of the detector. The signal from end plates and electron drift time allow us to reconstruct the trajectories of particles. The *TPC* detector provides us with information about the energy loss of particles $\left(\frac{dE}{dx}\right)$. Information about energy loss is important for particle identification. The Bethe-Bloch formula describes how mean energy loss is dependent on the velocity of the studied particle. Bethe-Bloch formula is described by the equation:

$$\left\langle \frac{dE}{dx} \right\rangle = \frac{C_1}{\beta} \left(\ln \left(C_2 \beta^2 \gamma^2 \right) - \beta^2 + C_3 \right), \tag{2.1}$$

where:

- C_1, C_2, C_3 - parameters specific for every detector,
- $\beta = \frac{v}{c}$,
- γ - Lorentz factor.

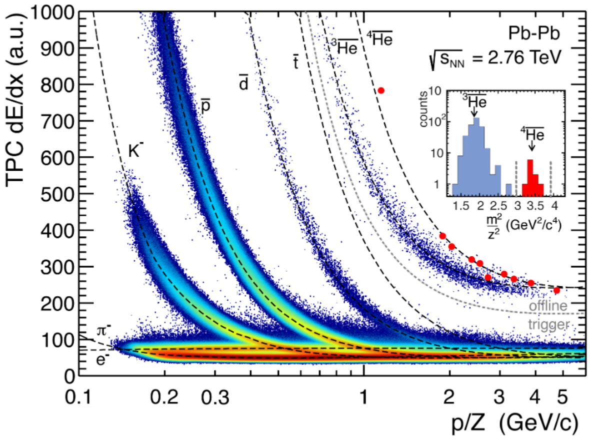

Figure 2.3: The TPC signal as a function of momentum divided by the electric charge of the particle [24].

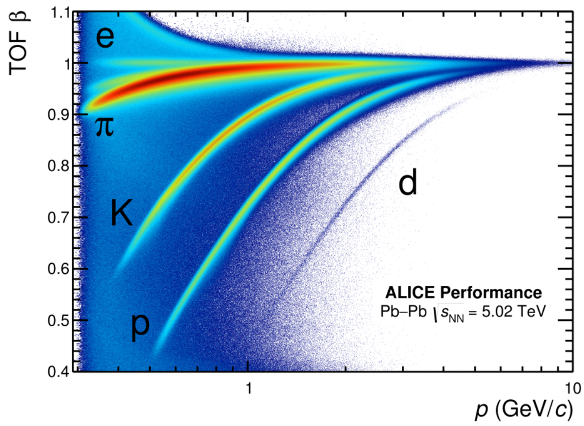

Figure 2.4: The TOF signal as a function of particle momentum [24].

2.3.4. Time-of-Flight (TOF)

The *TOF* detector provides us with information about *Time-Of-Flight*. Using *Time-Of-Flight* and particle trajectory, we are able to calculate velocity. We need to get distance, which is obtained from the *TPC* detector, and time, which is acquired from *TOF* and *T0* [22] detectors. After obtaining information about velocity, we are able to calculate mass from momentum. The *TOF* detector is therefore used to determine the mass of a studied particle. Figure **??** shows *TPC* as a function of momentum divided by the electric charge of the particle and *TOF* as a function of particle momentum.

2.4. GRID

The Worldwide LHC Computing Grid (WLCG) is a project linking computer centers from more than 40 countries worldwide. Its purpose is to enable the storage, distribution, and analysis of data from CERN [7]. GRID makes this possible for researchers by using about 1.4 million computer cores and 1.5 exabytes of storage. This allows real-time access and data processing from the LHC for physicists working around the world at CERN. When this thesis was written, global transfer rates exceeded 260 GB/s [23]. Figure 2.5 represents a map of GRID sites worldwide. Green dots indicate the sites that are running jobs.

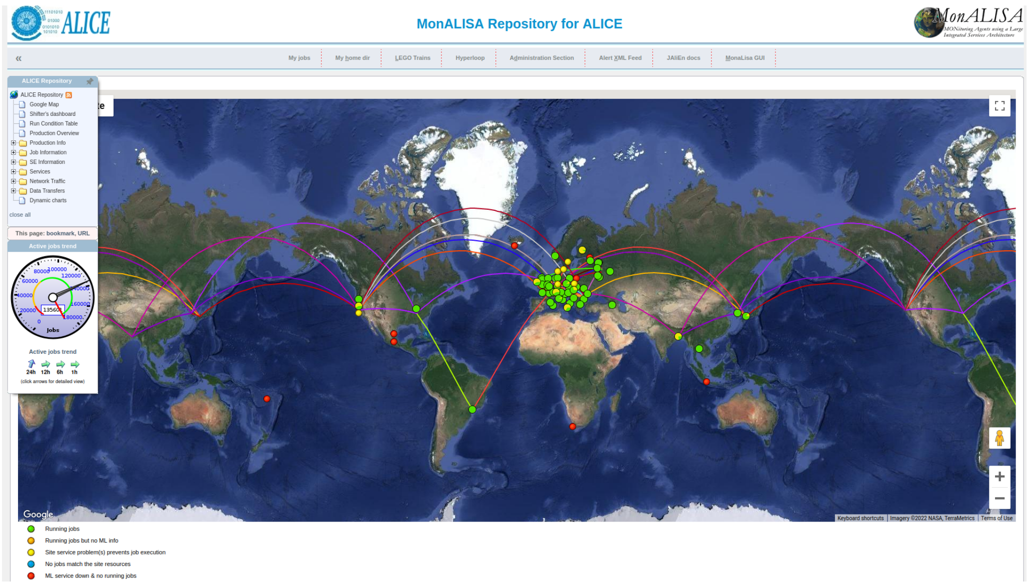

Figure 2.5: A map of GRID sites around the world.

Chapter 3

Software environment

3.1. Introduction to O^2 the framework

Long Shutdown 2 (LS2) [25] was the period from December 2018 to April 2022, and it was dedicated to maintaining and upgrading the LHC and accelerator complexes at CERN. During LS2, the heavy ion rate has been increased by five times up to 50 kHz. The high latency of the gas detector – TPC – made it impossible to adhere to the triggered acquisition mode used up to that point [26]. The ALICE detector has undergone a series of upgrades that has allowed it to acquire data continuously. Thus, it is designed in a manner that maximizes data volume reduction during data collection. Original raw data is replaced by O^2 system with compressed data after online partial calibration and reconstruction. New ALICE O^2 software was necessary to implement for Run 3 and Run 4 and it is a software that contains a sufficient framework for analyzing new data. It provides the framework needed for reconstruction and calibration for ALICE experiment [27]. The framework is built on C++ 17. In the future, there are plans to move to C++ 20 and 23, but because of ROOT [28] limitations, it is not yet possible.

3.2. The O^2 data format

A new data storage paradigm using flat tables has emerged with the new software. Each row refers to a different physical object, for example, a track, and each column refers to a different physical measurement. Created tables are Apache Arrow based [29]. Data used in Run 3 and Run 4 is organized as a structure of arrays. Arrays can refer to each other via Index Columns and are often joined or tied through an Index Table in order to enlarge the amount of available information necessary for analysis. Declarative programming, used in O^2, enables optimization, without implementing programming in explicit steps. Data is piped through a set of connected workflows and stays in their shared memory. Figure 3.1 shows the functional flow of the O^2 computing system.

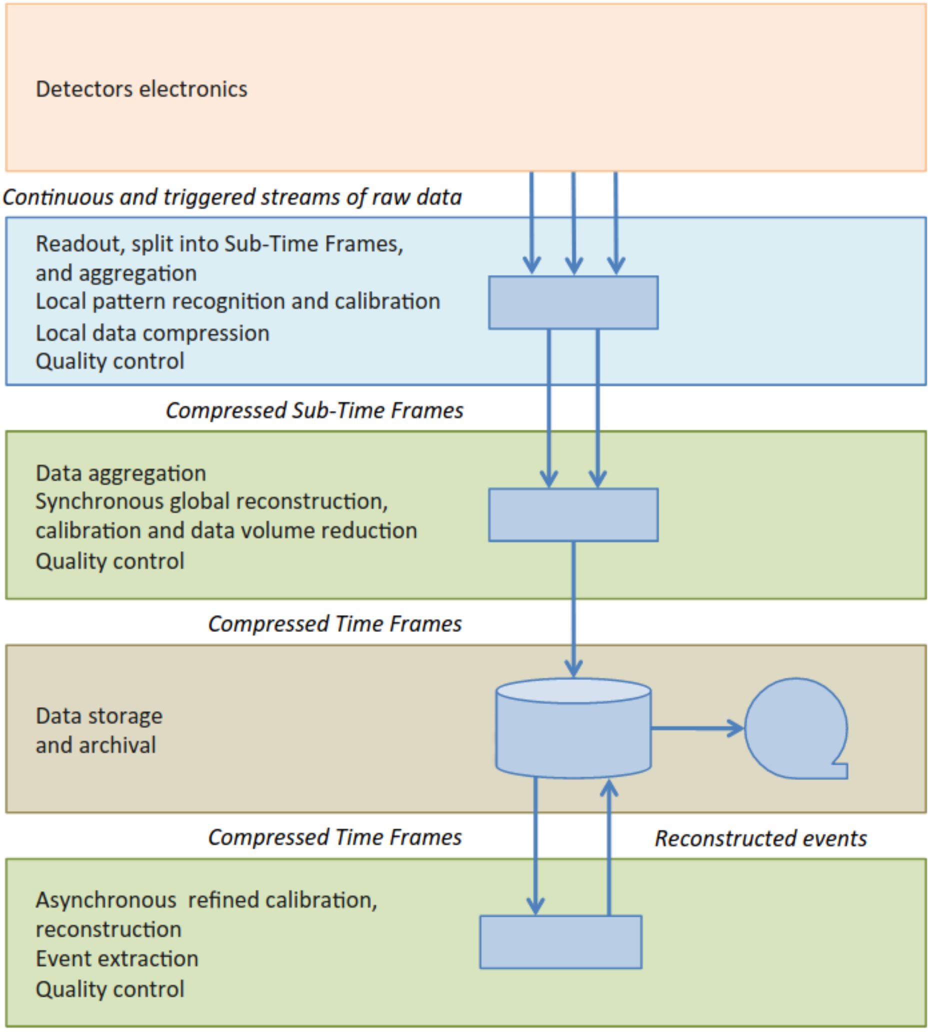

Figure 3.1: Functional flow of the O^2 computing system [30].

The continuous readout used in the detectors is a considerable change from the previously existing practice. Data is collected continuously through several continuous streams, and dedicated time markers are used to allow the data to be broken down into segments called Time Frames (TF).

3.3. FemtoWorld – the new O^2 module

The code used for data analysis in previous software (AliPhysics) cannot be used in O^2 software. It was therefore necessary to develop a large amount of code to make it possible to perform the set analysis. Due to the constant development of the new software, this required writing code from scratch.

As a base of the FemtoWorld software, I used the June 2022 version of the FemtoDream folder, located already in the O^2 tree. The FemtoDream folder is being developed by a group working at the Technical University of Munich (TUM). I used the code obtained from the FemtoDream folder to learn the O^2 software. Due to the fact that the two groups had different goals and contact was not frequent enough to inform each other of every change in the code, it was decided to create a separate folder in the O^2 tree for the WUT team - FemtoWorld [31]. I have developed documentation for the O^2 software, which can be found on my repository on GitHub [32]. I also took part in organizing the tutorial with Luca Barioglio and Maja Kabus on 03.08.2022 [33].
In common with any other directory in the O^2 tree, the FemtoWorld folder contains four subfolders:

- *Core* – which includes code, which compiles into libraries,
- *DataModel* – which contains headers that define derived data tables,
- *TableProducer* – which includes tasks which produce tables (defined in the *DataModel* directory),
- *Tasks* – which contains analysis tasks.

Figure 3.2 represents the diagram of the FemtoWorld analysis framework in the O^2 software.

Production of derived data

As outlined in previous chapters, the paradigm of the O^2 computational model is to greatly decrease the volume of used data. Therefore, the data that is not necessary is removed from the raw data used for this analysis, and thus derived data is created. To achieve this, I wrote a task *TableProducer/femtoWorldProducerTask.cxx* that created tables with data in the format defined in the *DataModel/FemtoWorldDerived.h* file.

Φ meson reconstruction

Due to the short lifetime of Φ mesons, only ~$1.5 \cdot 10^{-22}$ s [34], they do not reach detectors. They decay via strong force. Information on Φ mesons is being reconstructed from their daughters. Φ meson most frequently decays into mesons K^+ and K^-, with branching ratio - $BR_{\Phi \to K^+K^-}$ =

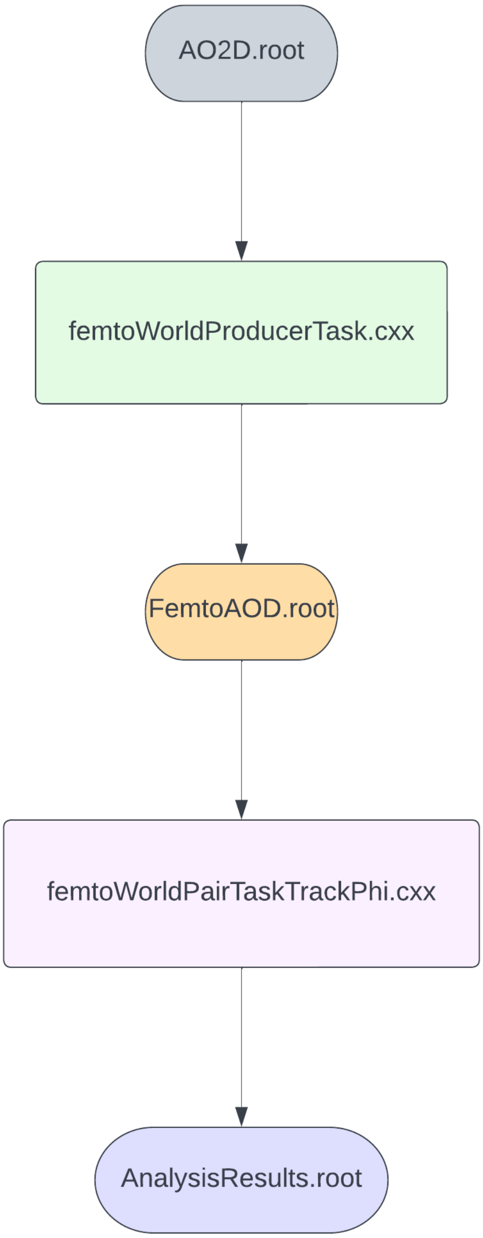

Figure 3.2: Diagram of FemtoWorld analysis framework in the O^2 software.

$(49.1 \pm 0.5)\%$ [35]. To reconstruct Φ meson properties, such as azimuthal angle φ, pseudorapidity η, and transverse momentum p_T I have used Lorentz vectors. In order to use this data for further analysis, it is necessary to save it to a table. For this reason, I have done the Φ meson reconstruction phase at the derived data production stage.

3.4. Hyperloop train system

The Hyperloop train system [36] is used to submit your analysis in a train to the GRID. Hyperloop is used for testing and running analysis on AliEn [37]. It is based on the LEGO train system, which was the system used and developed in the previous runs (Run 1 and Run 2 data) [38].

The Hyperloop train system has been designed to support the ALICE O^2 software. Several improvements have been made since AliPhysics. The most significant of these are unified train run submission, wagon and dataset bookkeeping, automatic wagon testing, and automatic train compilation and submission. Figure 3.3 shows the AliHyperloop page. Figure 3.4 shows the process of submitting a Hyperloop train run.

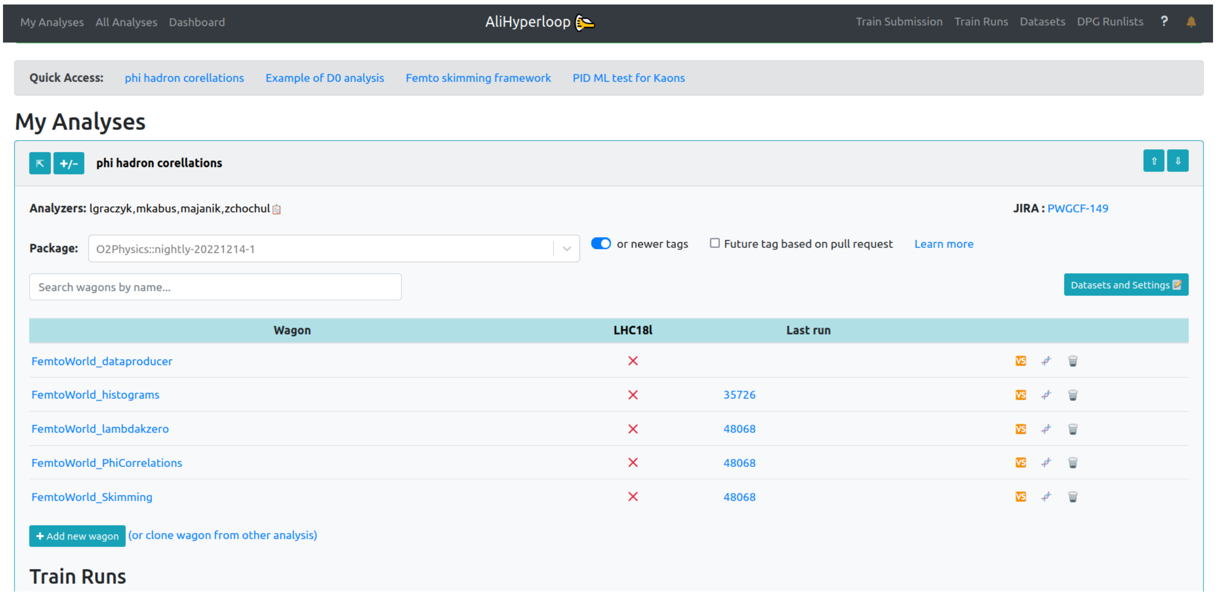

Figure 3.3: The AliHyperloop page [36].

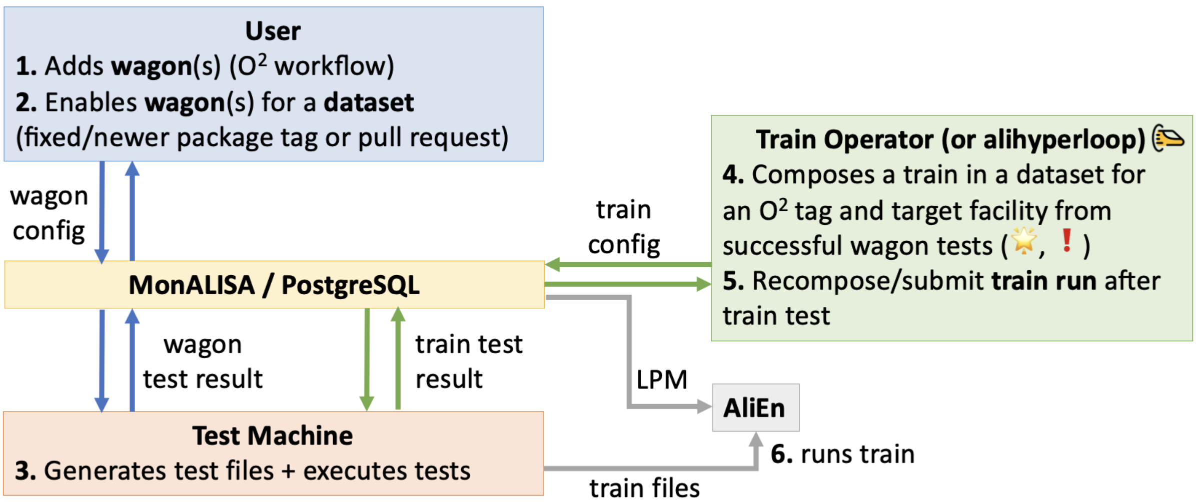

Figure 3.4: Process to submit a Hyperloop train run [39].

Chapter 4

Data analysis

4.1. Data sample

The data used in this analysis is from pp collisions recorded in 2018 (Run 2) at $\sqrt{s} = 13$ TeV, converted to the Run 3 data model. In the dataset collecting data from all collection periods of 2018 (LHC18bdefghijklmnop) alone, $5.1 \cdot 10^8$ events were registered. A minimum bias trigger was used. Figure 4.1 represents a multiplicity permille histogram obtained from the LHC18l dataset. V0M is a centrality estimator based on the sum of the amplitudes in the VZERO scintillators [40].

4.2. Proton candidate selection

Table 4.1 summarizes the selection criteria for protons. Only the most important parts of the selection procedure are described in more detail below.

The selection at the distance of the closest approach on both the beam plane (DCA_z) and transverse plane (DCA_{xy}) makes the number of secondary particles decrease. A cutoff on p_T at low momenta is being used in order to minimize the number of protons coming from the interactions of primary particles with the detector material. Selection on high p_T allows for increasing the purity of the selected particles. For the identification of particles, TPC (Time Projection Chamber) and TOF (Time Of Flight) detectors are used. For particles with momentum p<0.4 GeV/c, only the TPC detector is used for identification. PID in this momentum range is based on the n_σ method, it represents the number of standard deviations from the Bethe- Bloch curve. For momentum p>0.4 GeV/c, both the TPC and TOF detectors are used, using the $n_{\sigma,combined}$ method. The $n_{\sigma,combined}$ method means that one takes the root of the sum of the squares of the n_σ derived from the TPC curve and the TOF curve, as described by equation 4.1:

$$n_{\sigma,combined} = \sqrt{n^2_{\sigma,TOF} + n^2_{\sigma,TPC}}. \tag{4.1}$$

Figures 4.2 - 4.6 present the azimuthal angle φ, pseudorapidity η, transverse momentum p_T, TOF and TPC distributions for protons.

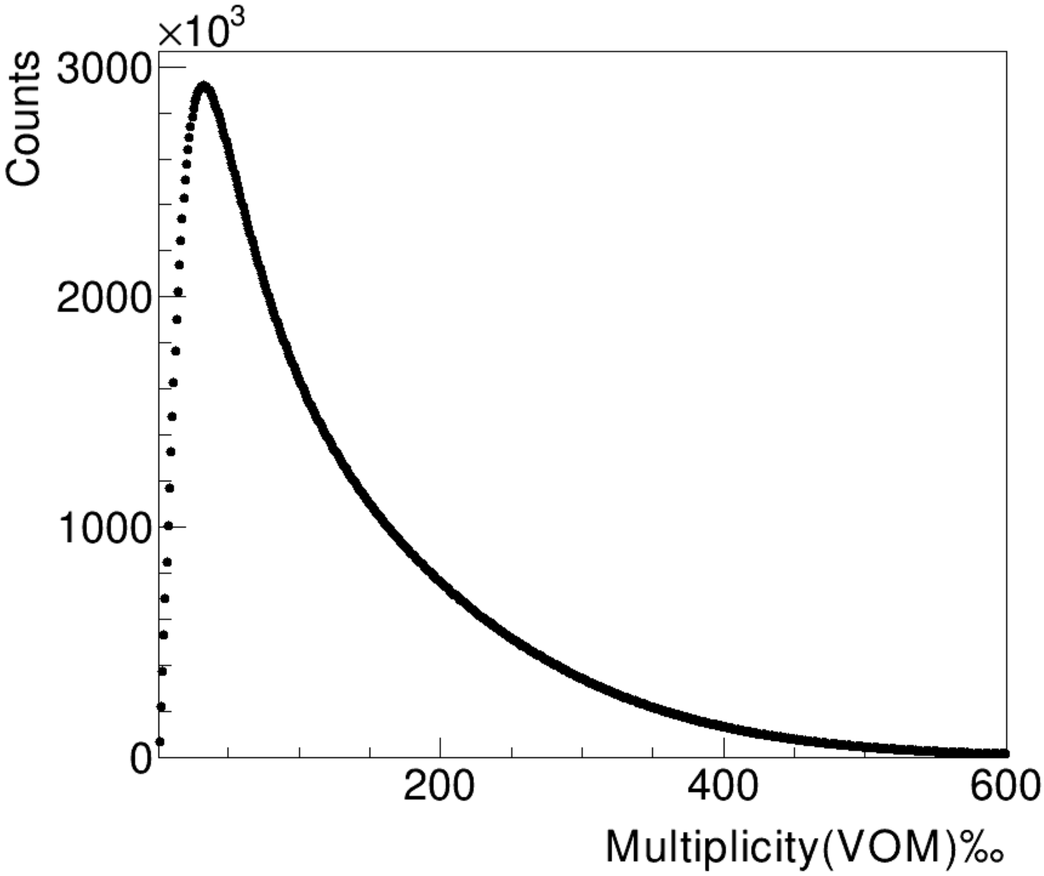

Figure 4.1: Multiplicity histogram for pp collisions registered at $\sqrt{s} = 13$ TeV.

Selection criteria	Value
Pseudorapidity	$\|\eta\| < 0.8$
Transverse momentum	$0.5\,\mathrm{GeV/c} < p_T < 4.0\,\mathrm{GeV/c}$
Crossed TPC pad rows	70
Number of TPC clasters	88
Distance of closest approach xy	$\|DCA_{xy}\| < 2.4\,\mathrm{cm}$
Distance of closest approach z	$\|DCA_z\| < 3.2\,\mathrm{cm}$
Particle identification	$\|n_{\sigma,TPC}\| < 3.0$ for $p < 0.5 GeV/c$
	$\|n_{\sigma,combined}\| < 3.0$ for $p > 0.5 GeV/c$

Table 4.1: Proton selection criteria.

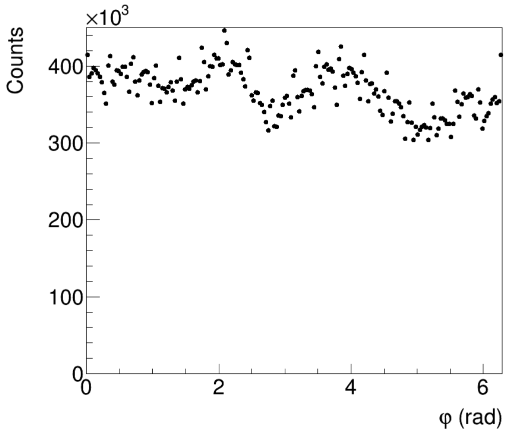

Figure 4.2: φ distribution for protons.

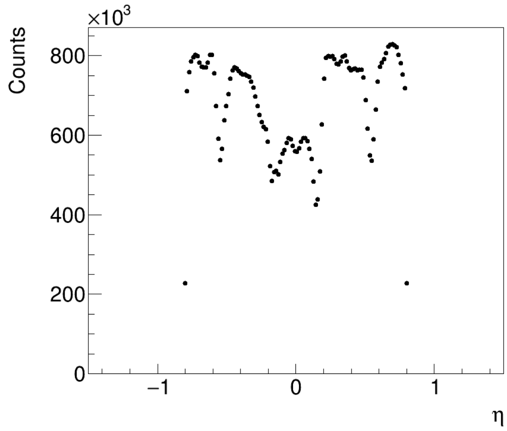

Figure 4.3: η distribution for protons.

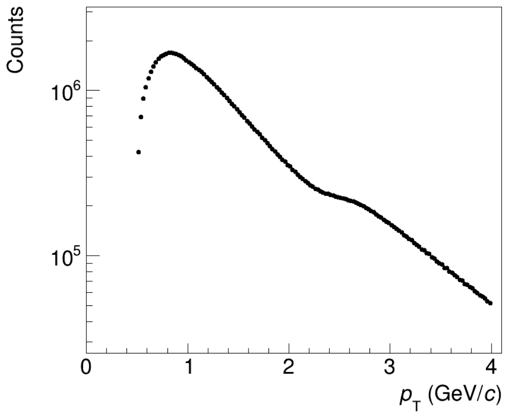

Figure 4.4: p_T distribution for protons.

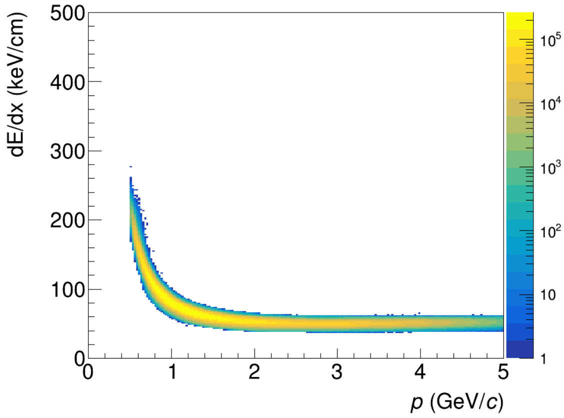

Figure 4.5: TPC vs p for protons.

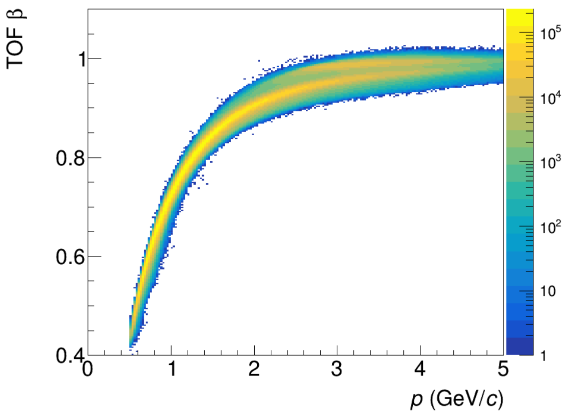

Figure 4.6: TOFβ vs p for protons.

Selection criteria	Value
Pseudorapidity	$\eta < 0.8$
Transverse momentum	$p_T > 0.15$ GeV/c and $p_T < 3.5$ GeV/c
Crossed TPC pad rows	70
Number of TPC clusters	88
Φ invariant mass	$1.011\text{GeV/c}^2 < M_{K^+K^-} < 1.027\text{GeV/c}^2$
Distance of closest approach xy	$\lvert DCA_{xy}\rvert < 2.4$ cm
Distance of closest approach z	$\lvert DCA_z\rvert < 3.2$ cm
Particle identification	$\lvert n_{\sigma,\text{TPC}}\rvert < 3.0$ for $p < 0.4$ GeV/c
	$\lvert n_{\sigma,\text{combined}}\rvert < 3.0$ for $p > 0.4$ GeV/c

Table 4.2: Kaon selection criteria.

4.3. Φ candidate selection

The Φ meson is a particle with a short lifetime ~$1.5 \cdot 10^{-22}$ s [34]. It most frequently decays into mesons K^+ and K^- with branching ratio - $BR_{\Phi\to K^+K^-} = (49.1 \pm 0.5)\%$ [35].

Kaon candidate selection
Since the most common Φ meson decay channel is K^+ K^- ($BR_{\Phi\to K^+K^-} = (49.1\pm0.5)\%$ [35]), the key step in the accurate reconstruction of short-lived Φ mesons is the proper identification of kaons into which it decays. As a result of the short lifetime of Φ mesons, daughters of the Φ meson are considered primary particles.

Table 4.2 summarizes the selection criteria for kaons. The invariant mass selection allows the kaons into which the Φ meson decays to be distinguished from all of the kaons registered. With selection at the distance of the closest approximation on both the beam plane (DCA_z) and the transverse plane (DCA_{xy}), the number of primary particles increases. To identify kaons below p = 0.4 GeV/c, only the signal from the TPC detector is used. This is due to the fact that for low momentum a clear separation using the signal from TPC is possible, this changes as momentum increases and for higher momentum, a combined signal from TPC and TOF is used. Selection on high p_T ensures the purity of identified particles and selection for the low p_T minimizes the number of protons coming from interactions of primary particles with the detector material. Figures 4.7 - 4.11 represent φ, η, TPC vs p and TOF vs p for kaons, which passed the selection for the invariant mass for Φ meson. For now, there is no easy way to produce histograms for candidates for a Φ meson daughters separately.

Φ meson resonance
Reconstruction of Φ mesons is based on the invariant mass method of its daughters. Invariant mass is a physical quantity in relativistic physics that can describe a body or a system of bodies, that does not depend on the reference frame. In any reference system, intrinsic mass is determined

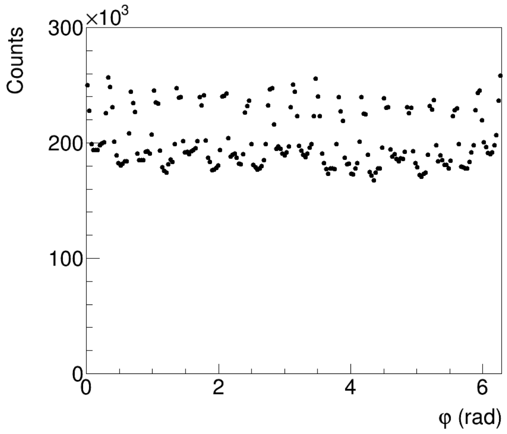

Figure 4.7: φ distribution for kaons, into which the Φ meson decays.

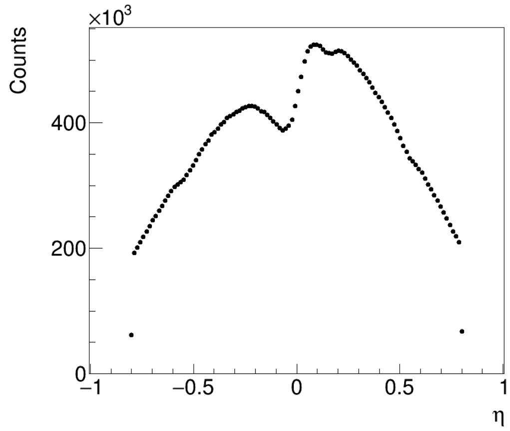

Figure 4.8: η distribution for kaons, into which the Φ meson decays.

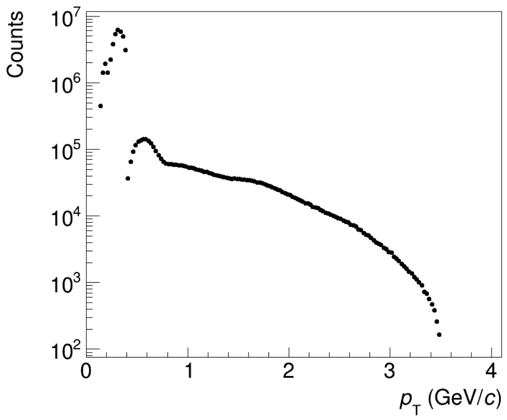

Figure 4.9: p_T distribution for kaons, into which the Φ meson decays.

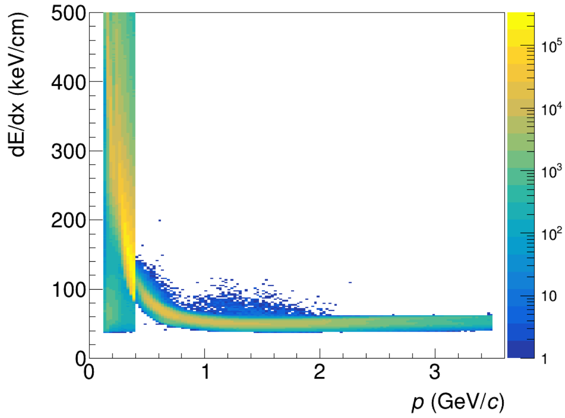

Figure 4.10: TPC vs p for kaons, into which the Φ meson decays.

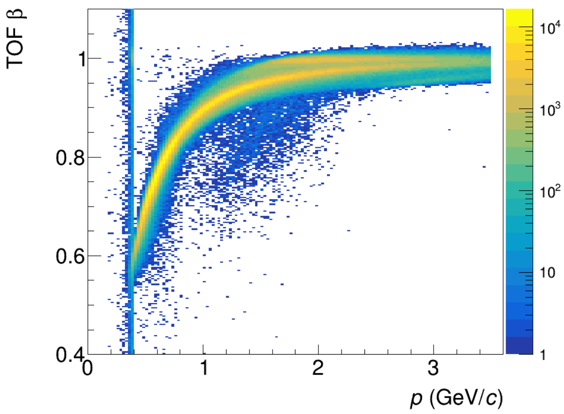

Figure 4.11: TOF β vs p for kaons., into which the Φ meson decays

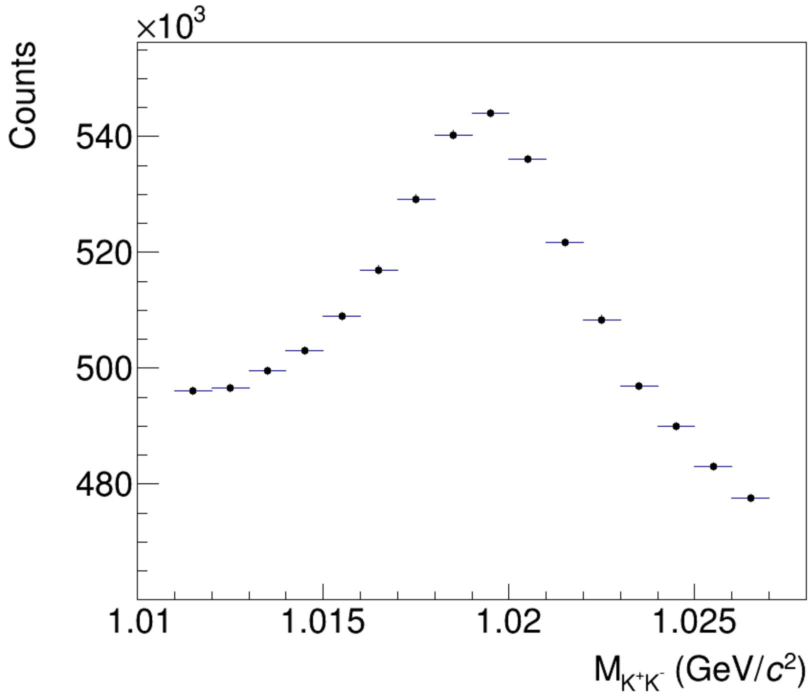

Figure 4.12: K^+K^- invariant mass distribution.

by the energies E and momentum p of all bodies:

$$M_{K^+K^-} = \frac{1}{c^2}\sqrt{\left(\sum_i E_i\right)^2 - \left|\sum_i \vec{p}_i\right|^2 c^2}. \tag{4.2}$$

Reconstructing particles that we cannot measure directly with detectors involves recording their decay products and looking for candidates for the particles into which they decay using the invariant mass distribution of potential daughters. Energy and momentum are conserved in the decay of a particle. If the entries on the histogram group around a certain value, we consider that we are observing a decay phenomenon. This value is the mass of the decaying particle. Figure 4.12 represents invariant mass for kaons.

Figure 4.13 represents invariant mass for kaons with fitted Lorentzian peak and polynomial. This particular figure was obtained locally on the pp collision data file recorded at energy $\sqrt{s}$ = 13 TeV in 2018. The pink and purple dashed lines in the figure show the ±2 σ and ±3 σ values respectively. Purity in the case was 0.64. It was determined by integrating the signal S and background B from -2 σ to 2 σ, and then dividing S by the sum of S+B.

Φ mesons are reconstructed with the use of Lorentz vectors. Lorentz vectors make it possible to obtain η, φ, and p_T values of Φ mesons derived from their daughters. Figures 4.14 - 4.16 represent φ, η and p_T for Φ mesons.

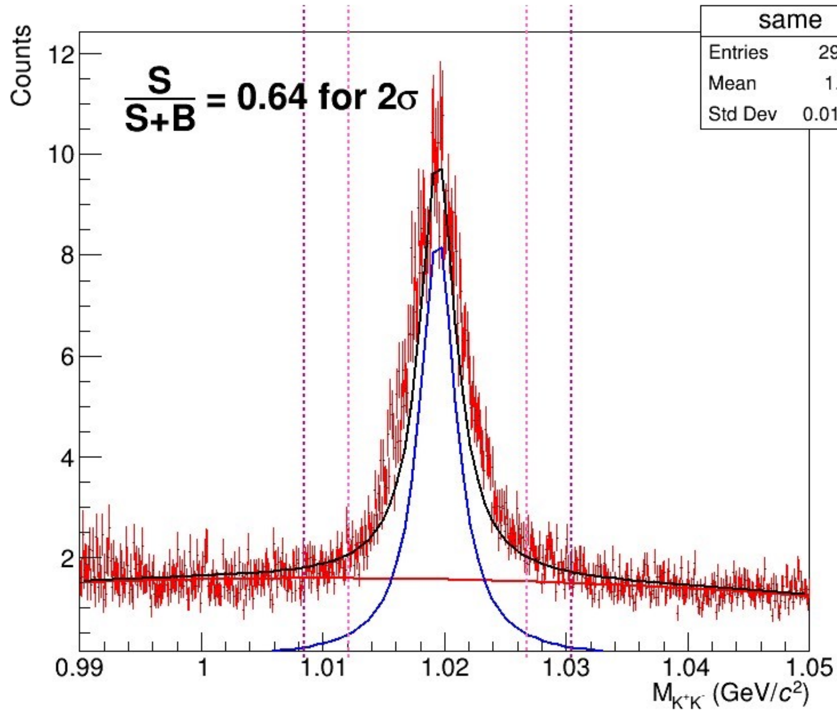

Figure 4.13: K^+K^- invariant mass distribution with fitted Lorentzian peak to the invariant mass peak and with polynomial fitted to the background.

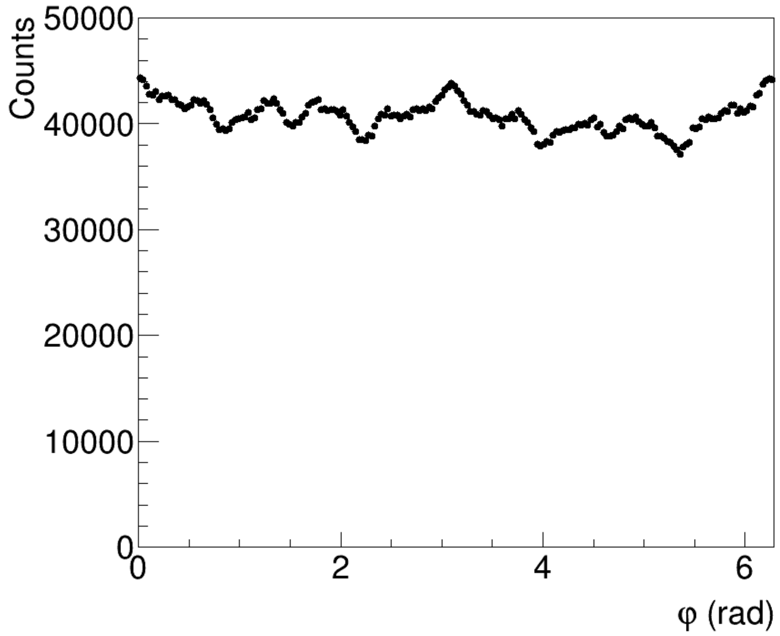

Figure 4.14: φ distribution for Φ mesons.

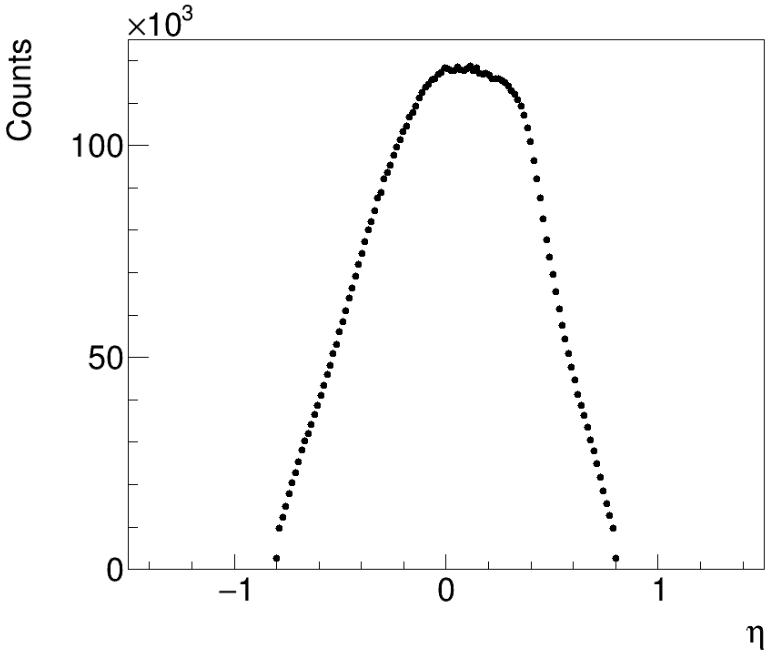

Figure 4.15: η for Φ mesons.

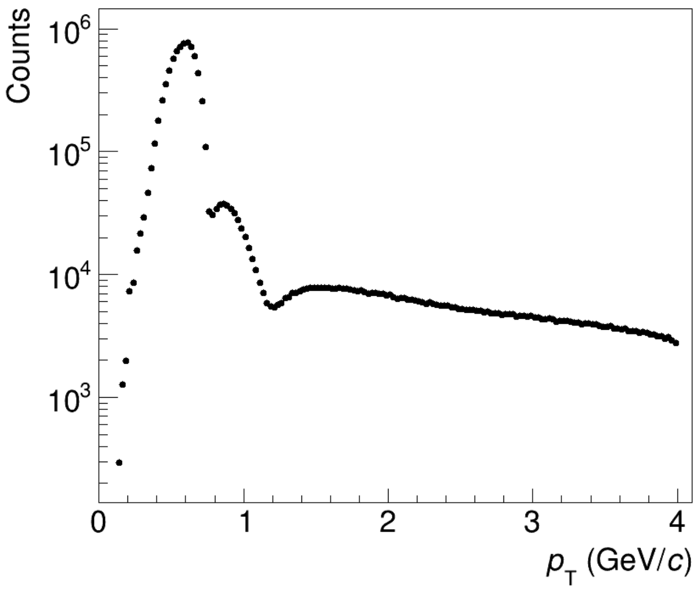

Figure 4.16: p_T for Φ mesons.

Chapter 5

Results

In this section, results are presented. Figures 5.1 and 5.4 represent $p - \Phi$ signal and background distribution, whereas figure 5.5 represents $p - \Phi$ angular correlation function. To increase the statistics, a mirroring method was used both on signal and background distributions. Signal and background distributions are symmetric with respect to the axis: $\eta = 0$, $\varphi = 0$, and $\varphi = \pi$. This method means that bins lying at the same distance from the symmetry axis were picked, and then the number of inputs was added up and averaged. Figures 5.2 and 5.3 represent projection on φ axis of the $p - \Phi$ signal and the background distribution, whereas figure 5.6 represents projection of the φ axis on angular correlation function.

The resulting angular correlation function does not show any of the predicted shapes. This is because the graph has too few inputs due to the small number of correlated $p - \Phi$ particle pairs. The number of pairs can also be increased by correlating more frequent particles with the Φ meson, for example, π mesons.

I have developed the code performing correlations of Φ with the identified hadron to include correlations with the π meson. In collisions, many more π mesons are produced than protons. The calculations were made with the hyperloop described in detail earlier in section 3.4. These calculations served as a sanity check of the code. The conclusion that can be drawn from the data obtained is that there is an error that makes us correlate fewer Φ mesons than there are actually in the data. Figures obtained from the $\pi - \Phi$ correlation analysis and their comparison with the $p - \Phi$ correlation are available in appendix A. Both analyses were calculated on the same LHC18l dataset, which is just a fraction of the data collected in 2018.

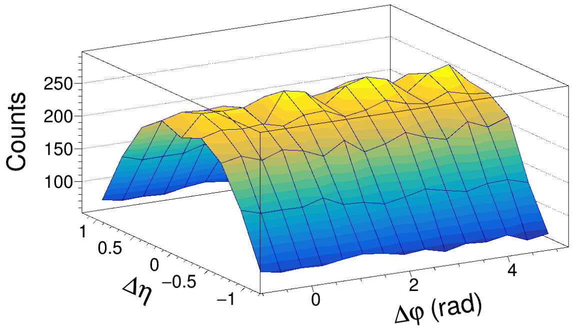

Figure 5.1: Signal distribution function for $p - \Phi$.

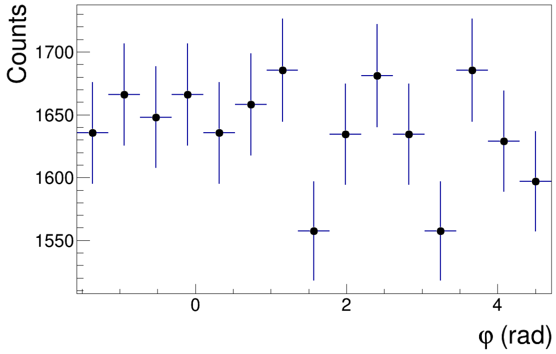

Figure 5.2: Signal distribution function for $p - \Phi$, projection.

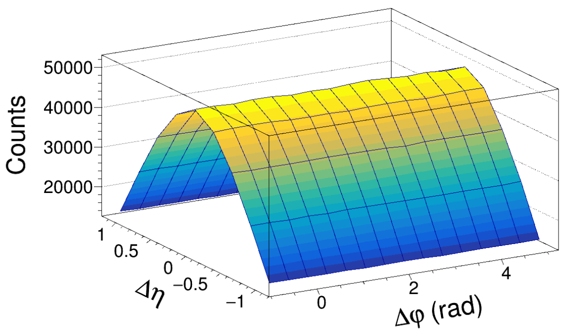

Figure 5.3: Background distribution function for $p - \Phi$.

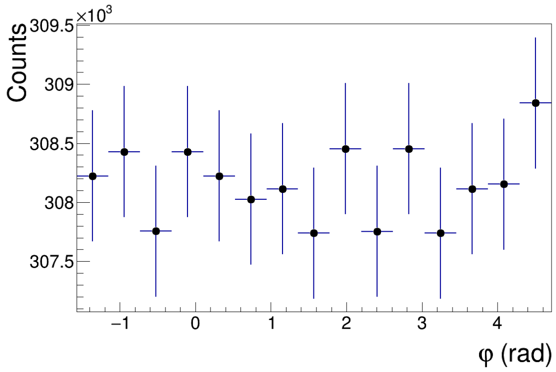

Figure 5.4: Background distribution function for $p - \Phi$, projection.

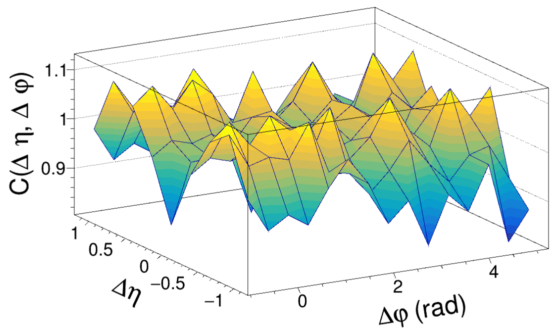

Figure 5.5: $p - \Phi$ angular correlation function.

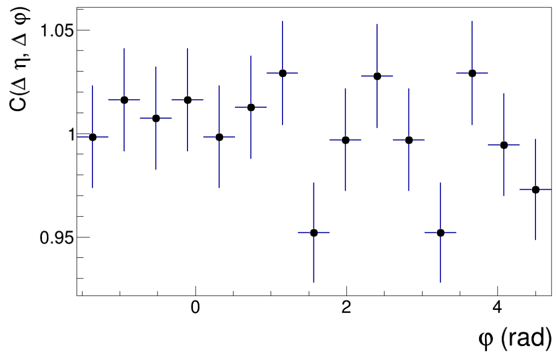

Figure 5.6: $p - \Phi$ angular correlation function, projection.

Chapter 6

Summary and conclusions

The aim of this thesis was to analyze $p - \Phi$ angular correlations in pp collisions recorded at the LHC at $\sqrt{s}$ = 13 TeV in the ALICE experiment at CERN. This work gives theoretical physicists working on the models measurement of the system that has never been studied before. The analysis of angular correlations $p - \Phi$ makes it possible to answer the question of whether the anticorrelation obtained for all the baryon-baryon and antibaryon-antibaryon pairs studied so far in the vicinity of $\Delta\eta\Delta\varphi$ = (0.0) is an effect influenced by mass.

Significant software development was required to perform angular correlation analysis in the new software used in the ALICE experiment – O^2. Working on the development of the FemtoWorld module required me to have many meetings with experts. During my two-month stay at CERN in the summer of 2022, I attended many meetings and tutorials organized by the collaboration. I also had the opportunity to see how the ALICE experiment works in person during the shifts at Run 3.

Working on the O^2 software required me to learn how to use GitHub. The ALICE collaboration granted me approval rights to part of the official repository on GitHub. I also presented the progress of my work at the ALICE staff meeting. I have also developed documentation for the O^2 software, which can be found on my repository on GitHub. I took part in organizing the tutorial with Luca Barioglio and Maja Kabus.

I was able to obtain the angular correlation function for $p - \Phi$. The shape of the correlation function does not resemble any of the expected shapes. The low number of inputs, which translates into a low number of pairs, is most likely due to a flaw in the O^2 software, at the pair creation stage. This is because we are creating fewer pairs than would result from how many particles we have. This issue will be addressed in the further development of the FemtoWorld module.

Bibliography

[1] I. C. Baianu et al. *Fundamentals of Physics and Nuclear Physics*. 2009.

[2] D. H. Perkins. *Introduction to high energy physics*. 1982.

[3] P. Foka and M. A. Janik. *An overview of experimental results from ultra-relativistic heavy-ion collisions at the CERN LHC: Bulk properties and dynamical evolution*. *Reviews in Physics*, 1:154–171, 2016.

[4] P. Foka and M. A. Janik. *An overview of experimental results from ultra-relativistic heavy-ion collisions at the CERN LHC: Hard probes*. *Rev. Phys.*, 1:172–194, 2016.

[5] B. Andersson, G. Gustafson, G. Ingelman, and T. Sjostrand. *Parton Fragmentation and String Dynamics*. *Phys. Rept.*, 97:31–145, 1983.

[6] Ł. K. Graczykowski. *What can we learn from femtoscopic and angular correlations of identified particles in ALICE?* *EPJ Web of Conferences*, 172:01007, 2018.

[7] Worldwide LHC Computing Grid: `https://wlcg.web.cern.ch/`, accessed: 02.11.2022.

[8] P. Nowakowski, P. Rokita, and Ł. Graczykowski. *Distributed simulation and visualization of the ALICE detector magnetic field*. *Computer Physics Communications*, 271:108206, 2022.

[9] M. Janik. *Two-particle correlations as a function of relative azimuthal angle and pseudorapidity in proton-proton collisions registered by the ALICE experiment* . CERN-THESIS-2014-339, 2014.

[10] Ł. K Graczykowski and M. A. Janik. Unfolding the effects of final-state interactions and quantum statistics in two-particle angular correlations. *Phys. Rev. C*, 104(5):054909, 2021.

[11] **ALICE Collaboration** J. Adam et al. *Insight into particle production mechanisms via angular correlations of identified particles in pp collisions at* $\sqrt{s} = 7$ *TeV*. *Eur. Phys. J. C*, 77(8):569, 2017. [Erratum: Eur.Phys.J.C 79, 998 (2019)].

[12] H. Aihara et al. *Study of baryon correlations in* e^+e^- *annihilation at 29 GeV*. *Phys. Rev. Lett.*, 57:3140–3143, Dec 1986.

[13] Our mission - CERN page: `https://home.cern/about/who-we-are/our-mission`, accessed: 20.10.2022.

[14] The CERN accelerator complex in 2019 - CERN Document Server: `https://cds.cern.ch/record/2684277`, accessed: 20.10.2022.

[15] The Large Hadron Collider - CERN page: `https://home.cern/science/accelerators/large-hadron-collider`, accessed: 20.10.2022.

[16] **ALICE Collaboration** K. Aamodt et al. *The ALICE experiment at the CERN LHC*. *JINST*, 3:S08002, 2008.

[17] ALICE Schematics - CERN Document Server: `https://cds.cern.ch/record/2263642`, accessed: 20.10.2022.

[18] **ALICE Collaboration**. *Performance of the ALICE VZERO system*. *Journal of Instrumentation*, 8(10):P10016, oct 2013.

[19] Domenico Colella. ALICE ITS: the Run 1 to Run 2 transition and recent operational experience. *PoS*, VERTEX2015:003, 2015.

[20] F. Reidt. *Upgrade of the ALICE ITS detector*. *Nucl. Instrum. Meth. A*, 1032:166632, 2022.

[21] J. et al Alme. *The ALICE TPC, a large 3-dimensional tracking device with fast readout for ultra-high multiplicity events*. *Nucl. Instrum. Meth. A*, 622:316–367, 2010.

[22] A. V. Veselovsky et al. *A fast electronic system of the T0 start trigger detector for the ALICE experiment*. *Instrum. Exp. Tech.*, 52:191–195, 2009.

[23] The Worldwide LHC Computing Grid (WLCG) - CERN page: `https://home.cern/science/computing/grid`, accessed: 02.11.2022.

[24] **ALICE Collaboration**. *The ALICE experiment – A journey through QCD*. 11 2022.

[25] LHC Report: Another run is over and LS2 has just begun... - CERN page: `https://home.cern/news/news/accelerators/lhc-report-another-run-over-and-ls2-has-just-begun`, accessed 06.01.2023.

[26] Eulisse G. et al. *Evolution of the ALICE Software Framework for Run 3*. *EPJ Web of Conferences*, 214:05010, 01 2019.

[27] Alice O2 software documentation: `https://aliceo2group.github.io/docs/`, accessed: 03.11.2022.

[28] ROOT data analysis framework page: `https://root.cern/`, accessed: 20.01.2023.

[29] G. Eulisse, presentation: *ALICE software framework for Run 3* `https://indico.jlab.org/event/519/contributions/9565/attachments/7746/10853/2022-05-eic-workshop.pdf`, accessed: 20.01.2023.

[30] P. Buncic, M. Krzewicki, and P. Vande Vyvre. *Technical Design Report for the Upgrade of the Online-Offline Computing System*. 4 2015.

[31] FemtoWorld directory - official ALICE O2 repository: `https://github.com/AliceO2Group/O2Physics/tree/master/PWGCF/FemtoWorld`, accessed: 19.01.2023.

[32] Alice O2 Run3 files and documentation - github repository: `https://github.com/zchochul/AliceO2`, accessed: 19.01.2023.

[33] O2 tutorial Hands on Session 1 - Femto tutorial: `https://indico.cern.ch/event/1088106/`, accessed: 19.01.2023.

[34] M. Tanabashi et al. *Review of Particle Physics*. *Phys. Rev. D*, 98:030001, Aug 2018.

[35] Φ meson (1020) - Particle Data Group page: `https://pdglive.lbl.gov/Particle.action?node=M004&init=0&home=MXXX005`, accessed 06.01.2023.

[36] AliHyperloop page: `https://alimonitor.cern.ch/hyperloop/`, accessed: 20.01.2023.

[37] **ALICE Collaboration** Saiz P. et al. *AliEn - ALICE environment on the GRID*. *Nucl. Instrum. Meth. A*, 502:437–440, 2003.

[38] The LEGO train system - ALICE Analysis Tutorial documentation: `https://alice-doc.github.io/alice-analysis-tutorial/analysis/lego.html`, accessed: 13.12.2022.

[39] R. Quishpe, J. F. Grosse-Oetringhaus, R. Cruceru, and C. Grigoras. *Hyperloop – The ALICE analysis train system for Run 3*. *PoS*, LHCP2021:250, 2021.

[40] D. d'Enterria and C. Loizides. *Progress in the Glauber model at collider energies*, 11 2020.

List of Figures

1.1 Definition of the polar angle θ and the azimuthal angle φ [8]. 15

1.2 Construction of the $\Delta\eta\Delta\varphi$ correlation function. Signal distribution (left), background distribution (middle), and correlation function (right) [9] 16

1.3 The components that comprise the angular correlation [10]. 17

1.4 Correlation function C($\Delta\eta$, $\Delta\varphi$) of unlike-sign and like-sign particles [9]. 17

1.5 Comparison to MC models: like-sign [11]. 18

1.6 Comparison to MC models: unlike-sign [11]. 18

2.1 Experiments and accelerators at CERN [14]. 20

2.2 3D ALICE schematics of ALICE detector after the upgrade for Run 3 [17]. 21

2.3 The TPC signal as a function of momentum divided by the electric charge of the particle [24]. . . 23

2.4 The TOF signal as a function of particle momentum [24]. 23

2.5 A map of GRID sites around the world. 24

3.1 Functional flow of the O^2 computing system [30]. 26

3.2 Diagram of FemtoWorld analysis framework in the O^2 software. 28

3.3 The AliHyperloop page [36]. 30

3.4 Process to submit a Hyperloop train run [39]. 30

4.1 Multiplicity histogram for pp collisions registered at $\sqrt{s}$ = 13 TeV. 32

4.2 φ distribution for protons. 33

4.3 η distribution for protons. 33

4.4 p_T distribution for protons. 33

4.5 TPC vs p for protons. 33

4.6 TOFβ vs p for protons. 33

4.7 φ distribution for kaons, into which the Φ meson decays. 35

4.8 η distribution for kaons, into which the Φ meson decays. 35

4.9 p_T distribution for kaons, into which the Φ meson decays. 35

4.10 TPC vs p for kaons, into which the Φ meson decays. 35

4.11 TOF β vs p for kaons., into which the Φ meson decays 35

4.12 K^+K^- invariant mass distribution. 36

4.13 K^+K^- invariant mass distribution with fitted Lorentzian peak to the invariant mass peak and with polynomial fitted to the background. 37

4.14 φ distribution for Φ mesons. 37

4.15 η for Φ mesons. 38

4.16 p_T for Φ mesons. 38

5.1 Signal distribution function for $p - \Phi$. 40

5.2 Signal distribution function for $p - \Phi$, projection. 40

5.3 Background distribution function for $p - \Phi$. 40

5.4 Background distribution function for $p - \Phi$, projection. 40

5.5 $p - \Phi$ angular correlation function. 40

5.6 $p - \Phi$ angular correlation function, projection. 40

A.1 TPC vs p for pions. 52

A.2 TOFβ vs p for pions. 52

A.3 φ distribution for pions. 52

A.4 η distribution for pions. 52

A.5 p_T distribution for pions. 52

A.6 Signal distribution function for $\pi - \Phi$. 53

A.7 Signal distribution function for $\pi - \Phi$, projection on the φ axis. 53

A.8 Background distribution function for $\pi - \Phi$. 53
A.9 Background distribution function for $\pi - \Phi$, projection on the φ axis. 53
A.10 $\pi - \Phi$ angular correlation function. 53
A.11 $\pi - \Phi$ angular correlation function, projection on the φ axis. 53
A.12 TPC vs p for proton. 54
A.13 TOFβ vs p for protons. 54
A.14 φ distribution for protons. 55
A.15 η distribution for protons. 55
A.16 p_T distribution for protons. 55
A.17 Signal distribution function for $p - \Phi$. 55
A.18 Signal distribution function for $p - \Phi$, projection on the φ axis. 55
A.19 Background distribution function for $p - \Phi$. 56
A.20 Background distribution function for $p - \Phi$, projection on the φ axis. 56
A.21 $p - \Phi$ angular correlation function. 56
A.22 $p - \Phi$ angular correlation function, projection on the φ axis. 56

List of Tables

4.1 Proton selection criteria. 32

4.2 Kaon selection criteria. 34

A.1 Pion selection criteria. 51

Appendix A

Comparison of angular correlation $\pi - \Phi$ with angular correlation $p - \Phi$

This section presents a comparison of the $\pi - \Phi$ angular correlation with the $p - \Phi$ angular correlation. Both $\pi - \Phi$ and $p - \Phi$ correlations were calculated on the LHC18l dataset. To increase the statistics, a mirroring method was used both on signal and background distributions. Signal and background distributions are symmetric with respect to the axis: $\eta = 0$, $\varphi = 0$, and $\varphi = \pi$. This method means that bins lying at the same distance from the symmetry axis were picked, and then the number of inputs was added up and averaged.

A.1. Angular correlation function for $\pi - \Phi$

Table A.1 summarizes the selection criteria for pions. The $\eta < 0.8$ selection was used. For particle momentum less than 0.5 GeV/c only TPC signal was used, whereas for the particle momentum greater than 0.5 GeV/c signal from both TPC and TOF was used for particle identification. As a range of momentum 0.5 GeV/c $< p_T <$ 4.0 GeV/c was used. Figures A.1 - A.5 represent the TPC and TOF, azimuthal angle φ, pseudorapidity η, and transverse momentum p_T, distributions for pions.

Figures A.6 and A.8 represent $\pi - \Phi$ signal and background distribution respectively, whereas figure A.10 represents $\pi - \Phi$ angular correlation function. Figures A.7, A.20 and A.11 represent projection on the φ axis signal distribution, background distribution and the correlation function respectively.

Selection criteria	Value
Pseudorapidity	$\eta < 0.8$
Transverse momentum	$p_T > 0.5$ GeV/c and $p_T < 4.0$ GeV/c
Crossed TPC pad rows	70
Number of TPC clusters	88
Distance of closest approach xy	$\lvert DCA_{xy}\rvert < 2.4$ cm
Distance of closest approach z	$\lvert DCA_{z}\rvert < 3.2$ cm
Particle identification	$\lvert n_{\sigma,\mathrm{TPC}}\rvert < 3.0$ for $p < 0.5$ GeV/c
	$\lvert n_{\sigma,\mathrm{combined}}\rvert < 3.0$ for $p > 0.5$ GeV/c

Table A.1: Pion selection criteria.

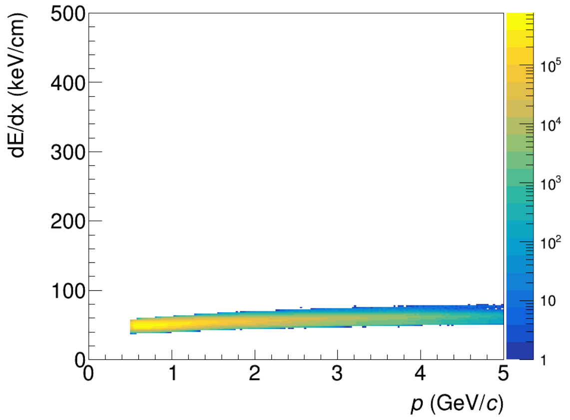

Figure A.1: TPC vs p for pions.

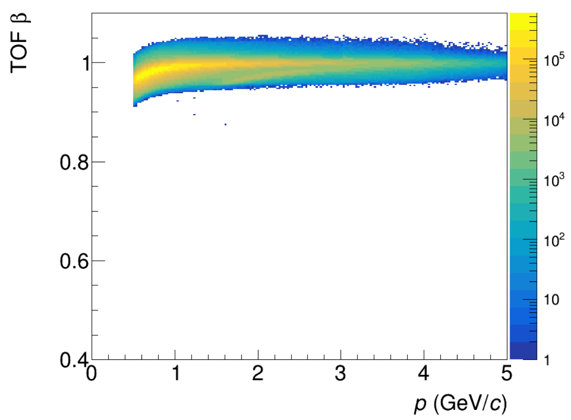

Figure A.2: TOFβ vs p for pions.

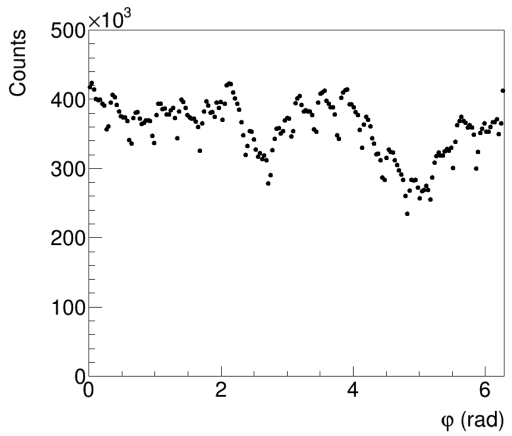

Figure A.3: φ distribution for pions.

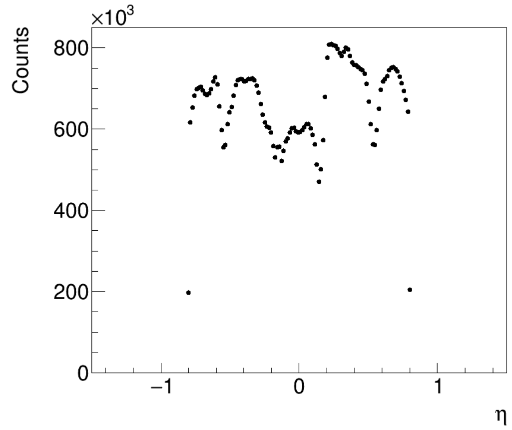

Figure A.4: η distribution for pions.

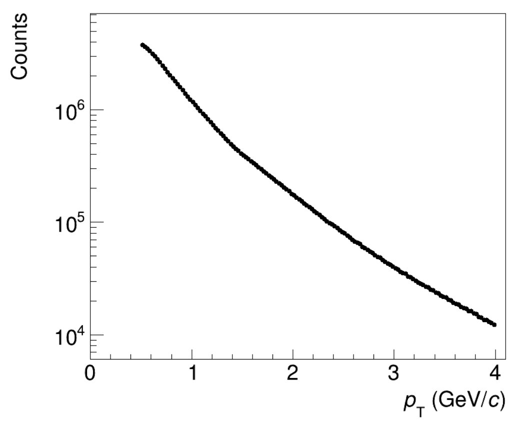

Figure A.5: p_T distribution for pions.

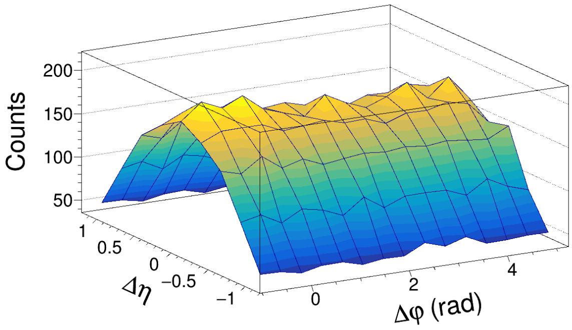

Figure A.6: Signal distribution function for $\pi - \Phi$.

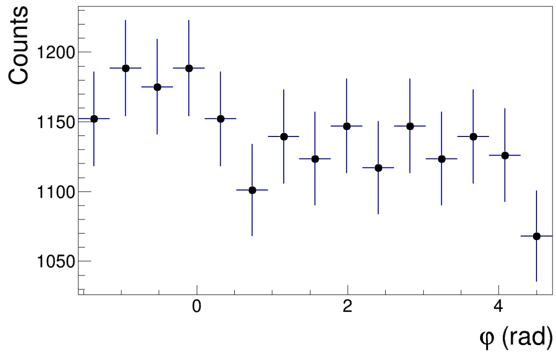

Figure A.7: Signal distribution function for $\pi - \Phi$, projection on the φ axis.

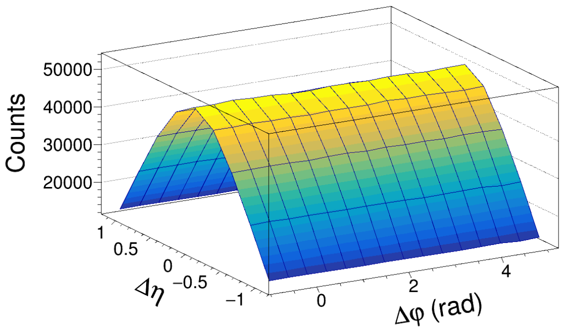

Figure A.8: Background distribution function for $\pi - \Phi$.

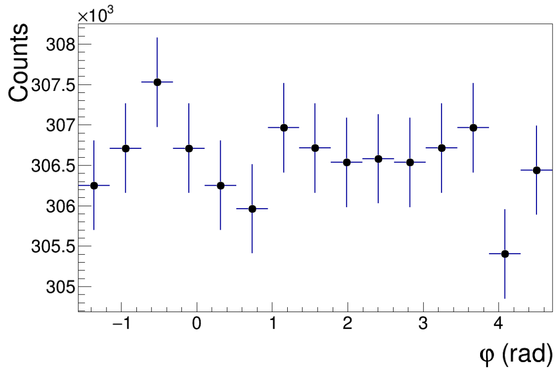

Figure A.9: Background distribution function for $\pi - \Phi$, projection on the φ axis.

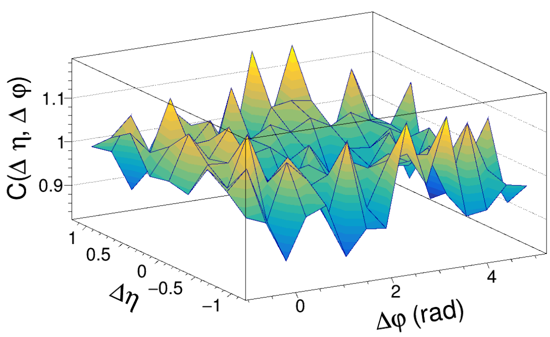

Figure A.10: $\pi - \Phi$ angular correlation function.

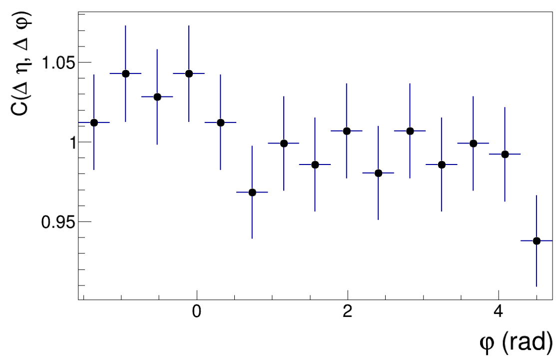

Figure A.11: $\pi - \Phi$ angular correlation function, projection on the φ axis.

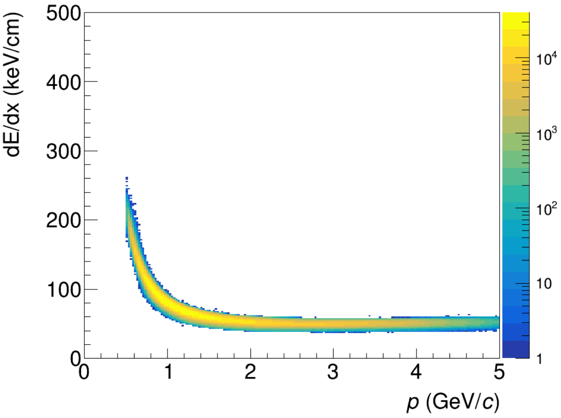

Figure A.12: TPC vs p for proton.

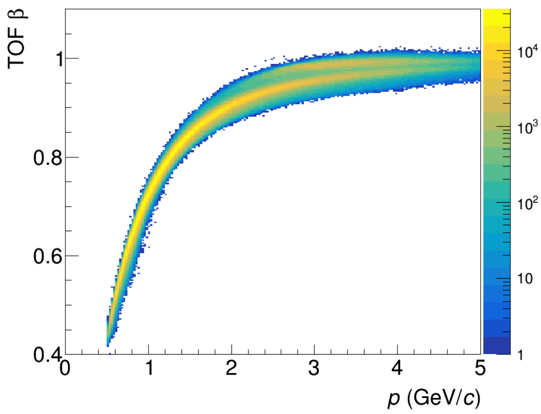

Figure A.13: TOFβ vs p for protons.

A.2. Angular correlation function for $p - \Phi$

The criteria for the selection of protons are described in table 4.1. Figures A.12 - A.16 represent the TPC and TOF, azimuthal angle φ, pseudorapidity η, and transverse momentum p_T, distributions for protons. Figures A.17 and A.19 represent $p - \Phi$ signal and background distribution respectively, whereas figure A.22 represents $p - \Phi$ angular correlation function. Figures A.17, A.19 and A.22 represent projection on the φ axis signal distribution, background distribution, and the correlation function respectively.

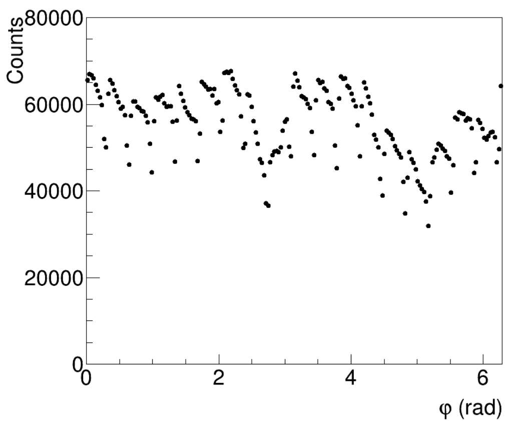

Figure A.14: φ distribution for protons.

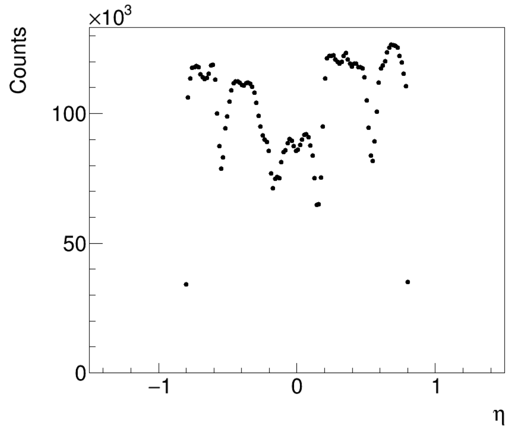

Figure A.15: η distribution for protons.

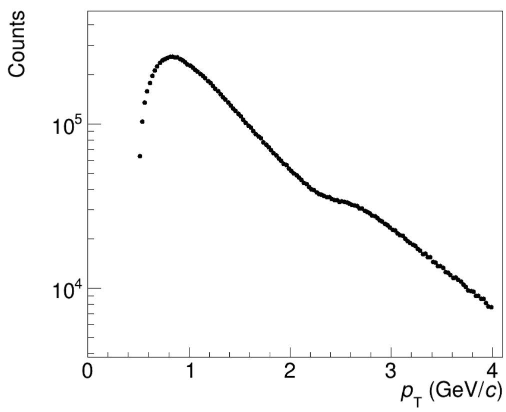

Figure A.16: p_T distribution for protons.

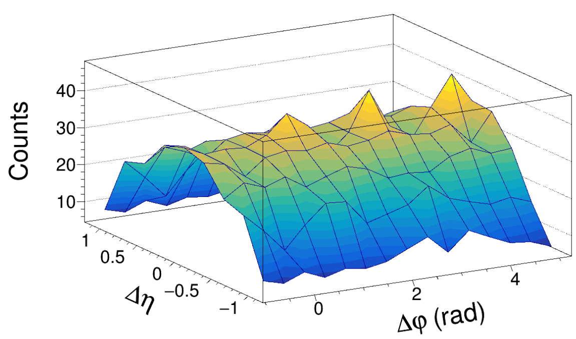

Figure A.17: Signal distribution function for $p - \Phi$.

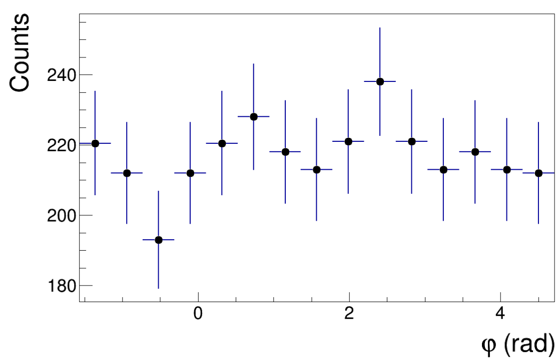

Figure A.18: Signal distribution function for $p{-}\Phi$, projection on the φ axis.

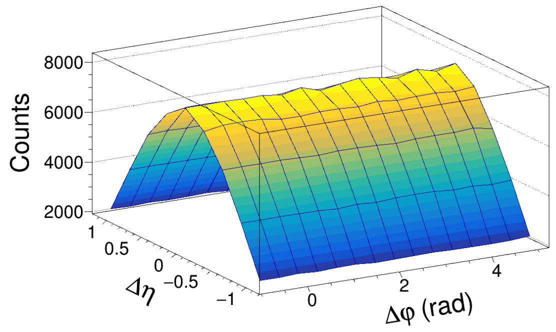

Figure A.19: Background distribution function for $p - \Phi$.

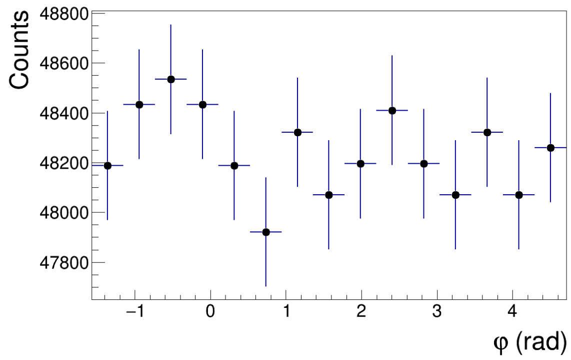

Figure A.20: Background distribution function for $p - \Phi$, projection on the φ axis.

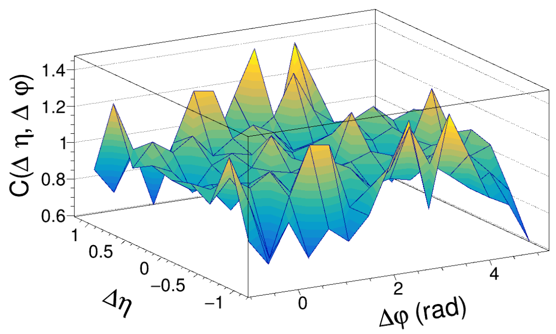

Figure A.21: $p - \Phi$ angular correlation function.

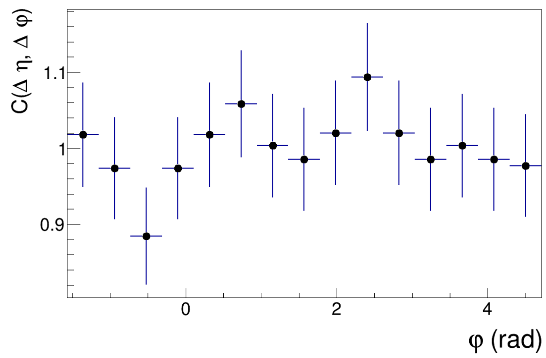

Figure A.22: $p - \Phi$ angular correlation function, projection on the φ axis.